Forest Ecology and Management 513 (2022) 120184

Contents lists available at ScienceDirect

Forest Ecology and Management

journal homepage: www.elsevier.com/locate/foreco

Uncovering forest dynamics using historical forest inventory data and Landsat time series

Viktor Myroniuk [a,*], David M. Bell [b], Matthew J. Gregory [c], Roman Vasylyshyn [a], Andrii Bilous [a]

[a] National University of Life and Environmental Sciences of Ukraine, Ukraine
[b] USDA Forest Service, Pacific Northwest Research Station, USA
[c] Oregon State University, Department of Forest Ecosystems and Society, USA

ARTICLE INFO

Keywords:
Forest change
Forest inventory
Growing stock volume
Imputation mapping
Nearest neighbor
Landsat
Phenology-linked data

ABSTRACT

While many countries regularly produce timely and accurate estimates for a range of forest attributes through national forest inventory programs, many have access to no such inventory or their inventory is discontinuous in space and time, such as a sample-based approach in Ukraine limited to two regional (Ivano-Frankivsk and Sumy) inventories conducted in 2008–2015 at a total area of 37,700 ha. This study addresses the extent to which limited historical forest inventory data may facilitate forest mapping efforts using dense Landsat time series (LTS) and mapping techniques (i.e., classification and imputation) to predict multiyear forest dynamics. We used the Continuous Change Detection and Classification (CCDC) segmentation approach to extract inter- and intra-annual trends in LTS and utilized these fitted trends as covariates in further modeling. We developed random forest (RF) classification models for forest mapping based on field data collection and LTS, and then generated yearly forest maps for 1990–2020. The RF model accuracies were high for both producer's and user's accuracy ($>0.93 \pm 0.04$). Based on yearly forest dynamics, we detected an increasing trend in forest loss during 2000–2010 and 2010–2020 in our regions. We used the gradient nearest neighbor (GNN) method to generate species presence (basal area (BA) ≥ 1.0 m^2 ha^{-1}) and growing stock volume (GSV) maps at the 30-m pixel level. Our nearest neighbor imputation models achieved better accuracies (Cohen's kappa > 0.4) for species that are prevalent within regions, occupy distinct geographical areas, and have higher plot BA abundance. To obtain estimates of species abundance with higher R^2, we used the GNN model with $k = 3$ nearest neighbors. Aggregating species based on similar environmental niche resulted in greater R^2 values of BA that varied within two regions from low (0.129 and 0.416) for a group of hardwood deciduous species to high (0.531 and 0.712) for coniferous species. The accuracy was systematically better at 5-km hexagonal level, thus we recommend using the maps at coarser aggregations. The study showed that forests accumulated more GSV in 1990–2000, albeit higher rates of GSV loss were observed during the two last decades. We attribute the spatial and temporal character of forest change to forestry activities in the past, the current age structure of forests, and afforestation of abandoned farmlands. We are aware that forecasting performance of the nearest neighbor imputation approach merits more detailed consideration as new forest inventory data are available.

1. Introduction

Intensive human activities (e.g., logging or infrastructure development) and natural disturbances (e.g., wildfires, insect infestation) along with climate change alter spatial pattern of landscapes, changing forest structure and biodiversity. The use of remote sensing technologies to examine the role of different disturbance agents in forest ecosystem dynamics over a range of spatial and temporal scales is well established (Bolton et al., 2019; Cohen et al., 2016; Hislop et al., 2019; Senf et al., 2017; Soulard et al., 2017). Better understanding of the historical context of forest dynamics promotes an improved strategy for sustainable forest management by linking multiple disturbance events and current structure of forests (Nguyen et al., 2018a). Moreover, mapping of forest structural attributes and their change provides data in support of long-term monitoring programs (Kennedy, Ohmann, et al., 2018; Matasci, Hermosilla, Wulder, White, Coops, Hobart, & Zald, 2018). Thus, spatially explicit information on forest cover dynamics collected retrospectively at suitable spatial scales provides a comprehensive

* Corresponding author at: 15 Heroiv Oborony St., Kyiv 03041, Ukraine.
E-mail address: victor.myroniuk@nubip.edu.ua (V. Myroniuk).

https://doi.org/10.1016/j.foreco.2022.120184
Received 9 November 2021; Received in revised form 18 March 2022; Accepted 21 March 2022
Available online 31 March 2022

framework for gaining insight regarding the accumulated effect of human interactions and natural factors on forest ecosystems resilience.

Retrospective analyses of forest dynamics has become a prominent component of modern forest monitoring as the availability of time series of satellite observations has increased (Banskota et al., 2014; Gómez et al., 2016). Recent advances in dense time-series processing using various temporal segmentation approaches (Brooks et al., 2014; Hermosilla et al., 2016; Huang et al., 2010; Kennedy et al., 2010; Zhu et al., 2020; Zhu & Woodcock, 2014) as well as successful implementation of these algorithms on the Google Earth Engine (GEE) cloud-based platform (Arévalo et al., 2020; Kennedy, Yang, et al., 2018) has improved the capacity to monitor rates of forest change over recent decades. Spectral trajectories of Landsat time series (LTS) have proven useful for detecting long-lasting and non-stand replacing disturbance (Bullock et al., 2020; Chen, 2021; Coops et al., 2020). Additionally, inclusion of disturbance history derived from LTS improves predictive performance of models, particularly by treating recovery as a subsequent process to disturbance (Matasci, Hermosilla, Wulder, White, Coops, Hobart, Bolton, et al., 2018; Nguyen et al., 2018a; Pflugmacher et al., 2012). Moreover, studies show potential to detect causal agents of forest disturbance using spectral change metrics (e.g., duration, magnitude) extracted using temporal segmentation algorithms (Nguyen et al., 2018a; Schroeder et al., 2017). A comprehensive analysis of forest monitoring technologies based on LTS is provided in Banskota et al. (2014).

The historically deep and data-rich Landsat archive has been recognized as an important resource for large-area forest monitoring. Benefiting from a free access policy, wide spatial coverage, moderate resolution of imagery (30–60 m for optical bands, 15 m for panchromatic band), and over four decades of data acquisition, Landsat imagery has found extensive application in various monitoring programs (Wulder et al., 2012, 2019). Over the last decade, LTS has been used as the basis for forest disturbance detection (Cohen et al., 2017; Nguyen et al., 2018a; Schroeder et al., 2017), and as a source to produce more stable spectral trajectories for forest classification (Hermosilla et al., 2018; Matsala, Bilous, Myroniuk, Holiaka, et al., 2021), including nearest neighbor imputation mapping (Bell et al., 2015, 2021; Davis et al., 2015; Kennedy, Ohmann, et al., 2018). Given the limitation for characterizing spectral variation caused by vegetation phenology using annual composites, the Continuous Change Detection and Classification (CCDC) algorithm has become extremely useful to derive intra-annual vegetation phenology and gradual inter-annual vegetation growth or abrupt change (Zhu & Woodcock, 2014). In addition to their ability to capture vegetation phenology, harmonic regression coefficients extracted from time series of spectral data have proven to be better predictors for key forest attributes than composite image variables. Particularly, Wilson et al (2018) achieved about two- to threefold increase in the coefficient of determination for models of continuous variables (i.e., number of trees, basal area, biomass) using harmonic models terms versus those using composite imagery. Further evaluation of seasonal composite and harmonic regression approaches identified better discrimination between forest types utilizing spectral trends and seasonality information quantified with harmonic inputs (Adams et al., 2020). Moreover, Derwin et al. (2020) showed that adding harmonic terms to spectral data and other explanatory variables (e.g., terrain variables) improves the performance of predictive models. The CCDC algorithm is also recommended as an effective means to deal with missed observations that appear due to the presence of snow or cloudiness (Awty-Carroll et al., 2019; Wilson et al., 2018). More recent publications have demonstrated the potential for improvement of the CCDC algorithm to detect even subtle changes in canopy (Ye, Rogan, Zhu, Hawbaker, et al., 2021) and near-real-time forest monitoring (Ye, Rogan, Zhu, & Eastman, 2021; Zhu et al., 2020). The increased demand on spatially-explicit information along with technological changes of data collection has led to wide application of LTS in support of forest inventories (Lister et al., 2020).

National forest inventory (NFI) is an important tool for collecting detailed information on forests, which supports decision making (Tomppo et al., 2010). The utility of sample-based inventory data is in addressing key monitoring questions regarding the status of the forest resources and developing national forest policies. Field data collected from sample plots provide detailed information on forest condition and structural attributes (i.e., age, species composition, growing volume, biomass, etc.), while repeated measurements of trees and site characteristics enable forest growth and change monitoring. Therefore, many countries have designed long-term national monitoring programs using sample-based forest inventory (Breidenbach et al., 2020). However, NFI programs were not initially designed to support mapped output, which is a key information need for most monitoring programs. Based on the seminal work of Tomppo (1990), many of these programs today use nearest neighbor modeling techniques to relate ground-based observations from a sparse network of sample plots to spectral properties from remotely sensed observations in order to produce wall-to-wall maps of forest characteristics (Chirici et al., 2016; Eskelson et al., 2009; McRoberts et al., 2010).

Within the forest inventory community, nearest neighbor imputation refers to a class of methods that estimate characteristics of a target pixel based on k reference observations (i.e., field plots) most similar in multivariate space of ancillary remote sensed, topographic, climatic, and other environmental variables (Eskelson et al., 2009; McRoberts, 2012; McRoberts et al., 2010). Nearest neighbor imputation has emerged as an effective technique for spatial prediction of forest attributes based on similarities between pixels associated with field plots and those without such association. This technique is recognized to be useful for spatial prediction because it is nonparametric and multivariate, and thus can be applied for simultaneously mapping multiple forest attributes (Henderson et al., 2014). The similarity between a target pixel and reference observations can be determined using common distance metrics (e.g., Euclidean), or quantified using a multivariate ordination technique such as canonical correlation analysis (used in most similar neighbor (Moeur & Stage, 1995)) or canonical correspondence analysis (used in gradient nearest neighbor (GNN) (Ohmann & Gregory, 2002)). An optimal choice of the number of neighbors (k) is always about the trade-off between accuracy and preservation of covariance among response variables. In particular, maps of forest characteristics produced with $k = 1$ nearest neighbor imputation model maintain existing combinations of attributes that can also be observed in the field (Ohmann et al., 2014). McRoberts (2009) demonstrated that covariance between forest attributes is preserved when only one nearest neighbor is used in imputation models. Conversely, nearest neighbor imputation with $k > 1$ usually minimizes the root mean square error of prediction (Hudak et al., 2008; Wilson et al., 2012) and higher values of k can be applied if there are large number of reference observations in the database (Eskelson et al., 2009).

Forest mapping using nearest neighbor imputation methods is commonly used in national- and regional-scale forest monitoring projects (Beaudoin et al., 2018; Chirici et al., 2020; Wilson et al., 2012). More recent applications of these techniques are associated with advances in image processing and availability of free satellite imagery that has created opportunities for integration of temporal segmentation methods with nearest neighbor imputation techniques. Such approaches provide an important insight into long-term monitoring of forest attribute dynamics. Specifically, Ohmann et al. (2012) first used yearly covariates derived from the LandTrendr temporal segmentation algorithm (Kennedy et al., 2010) as input to the GNN model to map yearly forest vegetation attributes in the Pacific Northwest USA. The LandTrendr temporal segmentation approach was also used to create temporally smoothed synthetic imagery, which was utilized to map forest biomass dynamics in Australia using nearest neighbor imputations (Nguyen et al., 2018b, 2020). Bell et al. (2021) incorporated an ensemble LandTrendr disturbance mapping algorithm (Cohen et al., 2018) to produce temporally smoothed LTS and assess trends in large live trees and snags using GNN imputation mapping. The Composite-to-Change (C2C) approach (Hermosilla et al., 2015) for image compositing was incorporated to predict forest structural attributes and aboveground biomass using nearest neighbor imputation in Canada (Matasci, Hermosilla, Wulder, White, Coops, Hobart, Bolton, et al., 2018; Zald et al., 2016).

Despite the wide application of information provided by national forest inventory internationally, the methodology of sample-based inventory in Ukraine is only under development. The majority of forests in Ukraine are state-owned, however these forests are managed by numerous state enterprises subordinated to various government institutions or self-governing bodies. The most reliable forest information is collected by the State Forest Resources Agency of Ukraine (73% of forests) while data provided by other agencies are infrequently updated. Satellite-based studies conducted in the Ukrainian Carpathians (Griffiths et al., 2014; Kuemmerle et al., 2009) and across Ukraine (Potapov et al., 2015) have revealed substantial changes in forest cover. Thus, without a systematic, coordinated national forest inventory, there is no authoritative or nationally consistent information about the state and dynamics of forests in Ukraine that can be used to inform forest management.

Preliminary results of regional-scale forest inventories that were conducted in Sumy and Ivano-Frankivsk oblasts (regions) during 2008–2015 and 2009–2015, respectively (Fig. 1), demonstrated great potential for supporting decision making, and updating the national forest statistics (Storozhuk & Polley, 2017). To the best of our knowledge, however, there were no applications in Ukraine to monitor changes of forest characteristics in a spatially explicit way using collected forest inventory (i.e., wall-to-wall mapping). For example, studies based on LTS in western Ukraine (Kuemmerle et al., 2009, 2011) and larger European territories including Ukraine (Griffiths et al., 2014; Potapov et al., 2015; Senf & Seidl, 2021) reported on forest changes, but not on forest characteristics such as species composition and growing stock volume (GSV). Conversely, the few existing applications of the nearest neighbor techniques to map forest characteristics within local test sites in Ukraine (Bilous et al., 2017; Matsala, Bilous, Myroniuk, Diachuk, et al., 2021) have not relied on data collected via a national forest inventory sampling design. Our principal goal here was to fill these gaps and examine the potential of characterizing forest dynamics

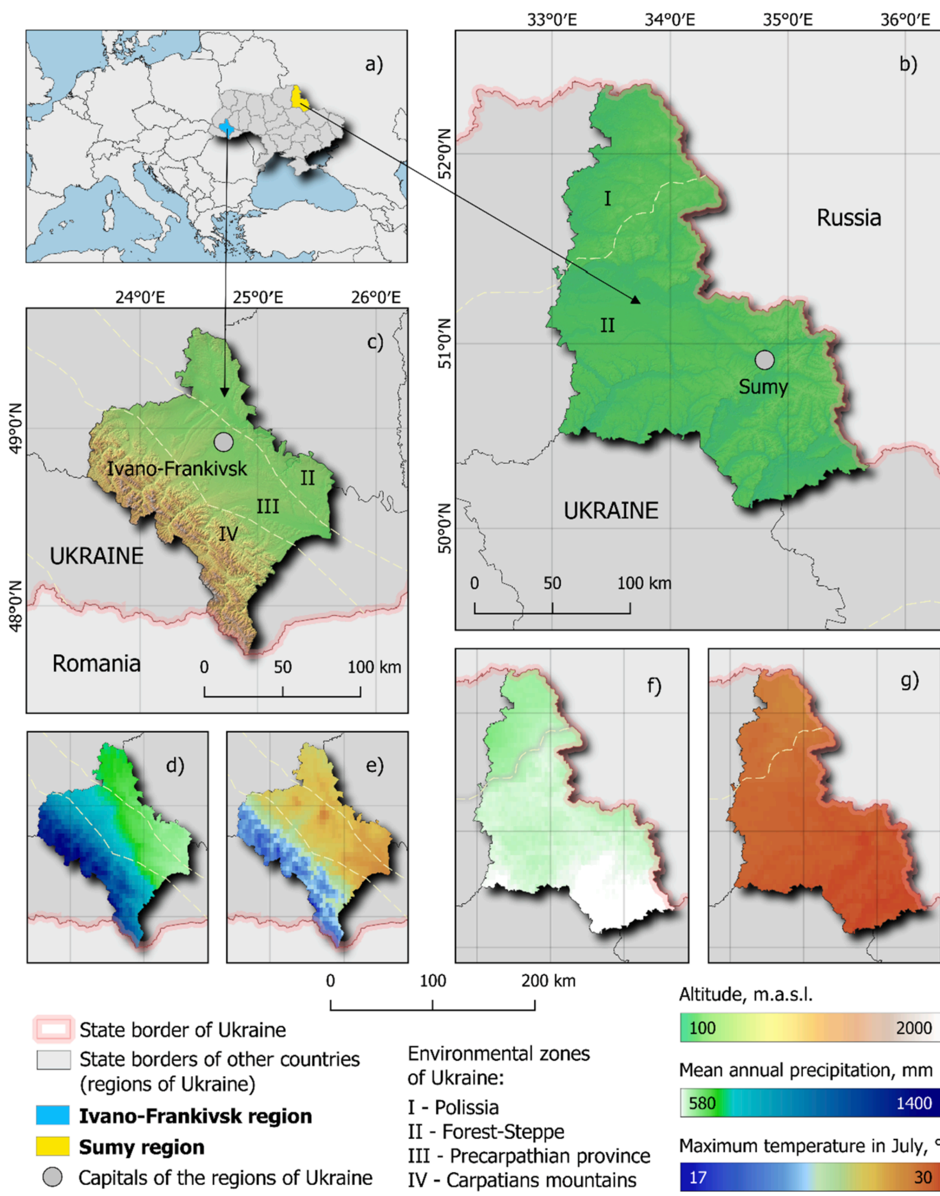

Fig. 1. Location of two study regions in Ukraine (a) overlaid with environmental gradients: (b), (c) elevation, m; (d), (f) mean annual precipitation, mm; (e), (g) maximum temperature in July, °C.

in two regions of Ukraine using recent forest inventory data collected via a national sampling design and LTS. Our specific objectives were threefold: 1) to assess long-term forest cover dynamics based on CCDC-fitted LTS; 2) to map spatial patterns of tree species distributions across the LTS time series using nearest neighbor imputation modeling techniques, and 3) to characterize spatial and temporal changes of GSV of forest stands. This regional-scale forest mapping effort may reveal trends in forest change that highlight the potential application of forest inventory data and remote sensing to provide spatially-explicit information, such as maps, in support of decision-making, as well as aggregating that data to support improving national forest policy and international forest reporting in Ukraine.

2. Materials and methods

2.1. Study area

This study is focused on two regions in Ukraine for which sample-based forest inventory data was available – the Ivano-Frankivsk region (13,900 km^2) in the west, and the Sumy region (23,800 km^2) in the east (Fig. 1). The Ivano-Frankivsk region has diverse topography including the Outer Eastern Carpathian Mountain range, which gradually lowers towards flatter lands to the east. The elevation of the territory varies from 230–400 m on flat land to 400–2061 m in the mountain range. The distribution of forest ecosystems in the region is associated with environmental zones (i.e, Carpathian Mountains, Precarpathian province, Forest-Steppe) as identified in Gensiruk (1992). Broad-leaved deciduous forests dominate in the eastern and central parts of the Ivano-Frankivsk region as well as the mountain foothills. European beech (*Fagus sylvatica* L.) forests dominate on low elevations of the mountain ranges, which are replaced uphill with mixed beech, silver fir (*Abies alba* L.), and Norway spruce (*Picea abies* L.) forests. The Sumy region belongs to the flat land Ukraine with elevation range of 100–246 m and two environmental zones – Polissia located in the northernmost part, and Forest-Steppe on the south. Scots pine-dominated (*Pinus sylvestris* L.) forest plantations contribute more to the forested area of the Polissia, while forest stands in the Forest-Steppe are preferentially composed of hardwood species, specifically common oak (*Querqus robur* L.), Norway maple (*Acer platanoides* L.), linden (*Tilia cordata* Mill.), and ash (*Fraxinus excelsior* L.). Unlike the Ivano-Frankivsk region where forests are concentrated in the Carpathian Mountains, forest cover of the Sumy region is heavily fragmented. Due to human activities in the past, larger patches of intact forests here were preserved in Polissia and along major river watersheds in Forest-Steppe. The gradient of climatic factors (i.e., distribution of annual precipitation and temperature) corresponds well with environmental zones and forest ecosystems' composition, although there is higher variation in the Ivano-Frankivsk region. The differences in environmental factors as well as spatial pattern and composition of forests associated with our two regions create the background for assessing the performance of remote sensing-based approaches for mapping forest cover dynamics.

2.2. Data

2.2.1. Forest inventory data

The field data for this research were acquired in the framework of regional forest inventories conducted during 2008–2015 in the Sumy region, and during 2009–2015 in the Ivano-Frankivsk region. The sampling design of the national forest inventory in Ukraine used a random allocation of circular sample plots within a systematic reference grid of 4.95 × 4.95 km (Fig. 2). Four fixed-area plots (500 m^2) were arranged into square-shaped clusters with 420 m spacing along each side of the cluster. The clusters were measured on five-panel annual rotation scheme, thus data in our study represents the completed first cycle of forest inventory, and the partially finished second cycle with plot re-measurements at the same locations. A more intensive (2.7 × 2.7 km) reference grid was applied during the first year of forest inventory within the Sumy region (2008) which was also used in 2013 re-measurements. The reduction of sampling intensity for other panels was imposed by financial constraints which led to the suspension of the national forest inventory program in Ukraine from 2015 to 2020.

Within each plot, all trees with diameter at breast height (1.3 m) greater than or equal to 6.0 cm were mapped by field crews and accurately measured for volume estimation. To calculate tree stem volumes, we used regional volume equations developed in Ukraine for major species based on tree diameter and height (Kashpor & Strochynskyi, 2013). Per hectare mean values of basal area (BA; m^2 ha^{-1}) and growing stock volume (GSV; m^3 ha^{-1}) were then summarized by each species at the stand level using individual tree data.

2.2.2. Reference data for modeling

All available forest inventory data were used for LTS classification to extract yearly forest/non-forest (FNF) maps using random forest (RF) classifier (Breiman, 2001) as described in section 2.3. Although the land

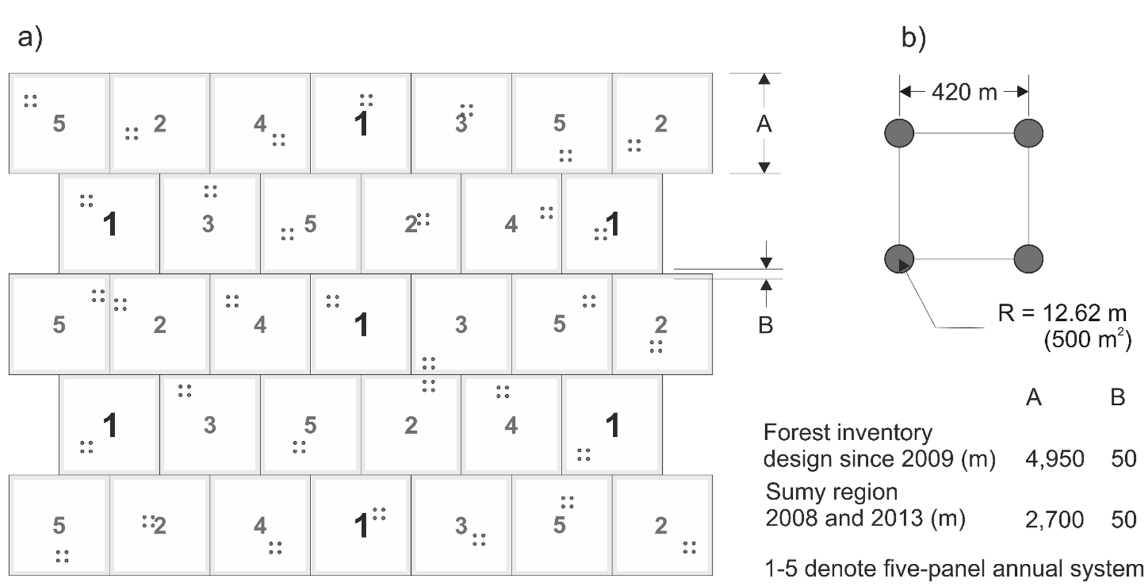

Fig. 2. Sampling frame for the regional forest inventories in Ukraine: (a) a systematic A × A square reference grid (B is no-sample buffer area); (b) cluster of four fixed-area sample plots (Storozhuk & Polley, 2017).

cover category was initially assigned to sample plots during the photo-interpretation phase of the regional forest inventories, we conducted an independent verification of the quality of forest and non-forest classes assignment using the Collect Earth plugin for Google Earth Pro designed to analyze high-resolution time series (Bey et al., 2016). The forest in our classification was defined as treed area > 0.3 ha with canopy cover > 30%. In addition, sample plots within the 2009 panel (464 and 769 plots within the Ivano-Frankivsk and Sumy regions, respectively) were visually interpreted for every fifth year between 1990 and 2020 using GEE-based LTS viewer (Arévalo et al., 2020), and incorporated in the study to test the accuracy of FNF maps using a cross-validation technique. For nearest neighbor imputation models (see section 2.4), we used only plots that were located on forested areas according to the developed forest maps (Fig. 3) (*sensu* Ohmann and Gregory 2002). Due to high level of forest fragmentation in Ukraine, mixed pixels potentially cause issues for imputation. For example, when a pixel straddles the boundary of an intact forest and a harvested forest, both pixels and plots are characterizing two distinct environments with differing spectral signatures, differing forest structure, and differing forest dynamics. Thus, we decided to also exclude plots that straddle different land cover categories. We also excluded any study plots with obvious mismatches between attributes and spectral data.

We spatially linked field plots with individual pixels to extract spectral and other explanatory variables used in modeling. Positional errors associated with field plot locations were less than 10 m (pers. comm. Vitaliy Storozhuk). No spatial smoothing was applied to account for potential misregistration between plot locations and pixels because a severely fragmented pattern of forest cover (especially within the Sumy region) might cause additional errors in reference data associated with edge effects. As a result of the more intensive reference grid applied in 2008 and 2013, the sample size for the Sumy region was higher. In this region, we used 9860 sample plots for FNF classification and 1196 plots for nearest neighbor imputation, while only 3202 and 838 sample plots were available in the Ivano-Frankivsk region for FNF classification and imputation, respectively.

2.2.3. Landsat time series and CCDC modeling

We utilized the GEE implementation of the CCDC algorithm (Zhu & Woodcock, 2014) to perform temporal segmentation of all available surface reflectance Landsat Collection 1 data from January 1, 1984 to January 1, 2021. Clouds, cloud shadows, and snow were filtered using the pixel quality attributes band generated from the CFMask algorithm (Foga et al., 2017), and fine-tuned with cloud-likelihood scoring algorithm available in GEE for top-of-atmosphere Landsat data, which utilizes the combination of brightness, temperature, and normalized snow index to get cloud scores. We applied a cloud score threshold of 40% in combination with CFMask that allowed us to improve the quality of LTS for mountainous areas of the Ivano-Frankivsk region which experience higher cloudiness and snow cover. In addition to the six original Landsat spectral bands, we added the first three primary components (brightness, greenness, and wetness) of the Tasseled-Cap transformation (TCT) (Crist & Cicone, 1984), the normalized burn ratio (NBR) (Key & Benson, 2006), and the Normalized Degradation Fraction Index (NDFI) indices (Souza et al., 2005), which were used in CCDC algorithm for temporal segmentation. Apart from CCDC segmentation, we did not use NBR or NDFI in further FNF or forest attribute modeling as they contributed less to models' performance (see section 2.3 for additional details). An interactive GEE time series viewer tool (Arévalo et al., 2020) was used to evaluate the performance of the CCDC algorithm with different parameters, however, we ultimately used default values (Appendix A, Table A1). We found that efforts to improve the sensitivity of the segmentation model to capture a subtle vegetation change (e.g., early stages of forest regrowth) yielded an excessively high number of segments that characterize identical land covers.

2.2.4. Ancillary environmental variables

We used additional environmental variables to improve the performance of the nearest neighbor imputation algorithm (Table 1). These environmental variables represent climatic and topographic drivers of forest structure and composition, which may either explain vegetation variation independent of the satellite imagery or alter the meaning of the imagery across differing geographies (Ohmann & Gregory, 2002). Gradients of the topographic features, specifically elevation and the topographic position index (TPI450) (Weiss, 2001), were extracted from 90-m spatial resolution Shuttle Radar Topography Mission (SRTM) digital elevation model. We also calculated mean annual precipitation

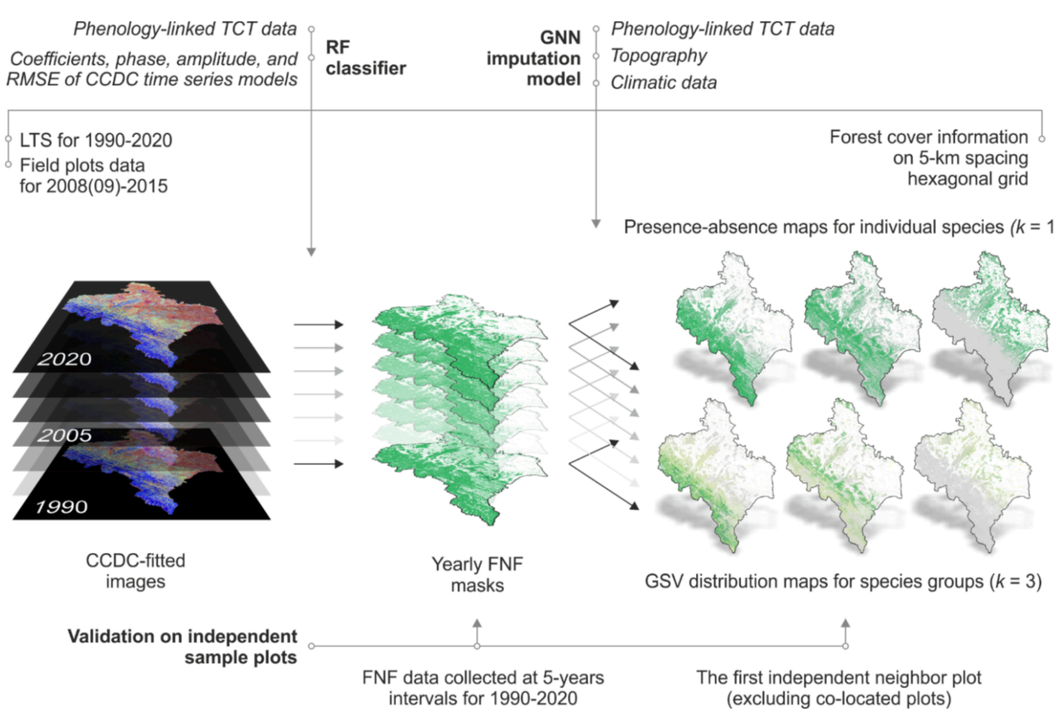

Fig. 3. Workflow for regional-scale mapping forest cover and nearest neighbor imputation of GSV using LTS.

Table 1
Geospatial data sets used in the study (a plus sign indicates that variable was used in corresponding model and a minus sign indicated it was not).

Variable type	Name	Description	RF	GNN
LTS	BRT	TCT brightness predicted using CCDC model for the 15th of April, June, October	+	+
	GRN	TCT greenness predicted using CCDC model for the 15th of April, June, October	+	+
	WET	TCT wetness predicted using CCDC model for the 15th of April, June, October	+	+
CCDC harmonic model	Coefficients	Intercept, slope, and harmonic terms of the harmonic regression models for BRT, GRN, WET	+	−
	RMSE	Root mean square error of the harmonic regression model	+	−
	Phase, amplitude	Phase and amplitude of the harmonic regression model	+	−
Topography	DEM	Elevation above sea level (m)	−	+
	TPI450	Topographic position index expressed as difference between the altitude and mean elevation within a 450-m neighborhood distance	−	+
Climate	ANNPREC	Mean annual precipitation (mm) extracted from TerraClimate dataset	−	+
	MAXTEMP	The 98th percentile of the maximum temperature in July (°C) extracted from TerraClimate dataset	−	+

(ANNPRE, mm) and 98th percentile of the maximum temperature in July (MAXTEMP, °C) from the global monthly TerraClimate data (Abatzoglou et al., 2018).

2.3. Mapping forested area

We tested several approaches to create FNF maps using information derived from CCDC (Zhu & Woodcock, 2014). We used: 1) model coefficients and derivations (e.g. phase and amplitude); 2) synthetic spectral bands created by fitting CCDC models at three dates; and 3) both covariates sets together. Since sample data had been collected only in 2008–2015, disagreement between reference land cover classes and CCDC segments affected model performance. Specifically, ambiguity of segmentation at the pixel level (Fig. 4b) which we refer to here as a missed segment break, or delays in detecting forest regrowth (Fig. 4c) can cause omission errors in forest masks for recent years (i.e., 2015–2020). While the steady change in spectral characteristics make sense from an ecological perspective, there may be a lot of variation in observer interpretation, leading to uncertainty in model performance. The ability to detect more gradual transition of land cover such as a grass-covered to forested was reported among the most obvious limitations of the CCDC approach (Brown et al., 2020). The two example pixels on Fig. 4 experienced transition from unforested to forested land cover type between 2008 and 2013 but were associated with non-forest segments. Given the mismatch between actual field observations and segmentation, the complete time series of per-pixel observation within the CCDC segment would be classified as a single land cover class. To address this issue, we applied a combined approach, which utilized coefficients of the time series models as inputs for RF classifier as well as predicted values of spectral bands extracted from the CCDC models.

We limited the list of spectral variables in our RF models to brightness, greenness, and wetness components of the TCT predicted for the start (April 15), middle (June 15), and end (October 15) of leaf-on period for the year of plot data collection. Based on previous experience in Ukraine, information on phenological differences of various vegetation improves the performance of land cover classification (Myroniuk et al., 2020). In addition, the CCDC harmonic terms are also associated with vegetation phenology (Arévalo et al., 2020) and were helpful in our study for disaggregating forest species from other types of vegetation (e.g., croplands, grasslands, shrubs, and riparian vegetation). We evaluated accuracy of the RF classification model in 1990–2020 using an independent validation data set (e.g., plots of 2009 panel interpreted for every fifth year in time range of 1990–2020) but did not find a way to enhance its predictive performance by introducing additional spectral indices (e.g., NBR and NDFI). The inclusion of topographic and climatic variables also did not improve the accuracy of FNF classification because no evidence of their influence on forest distribution in our regions was observed.

The reference data for the classification were available only for the years of field data collection in the Sumy (2008–2015) and Ivano-Frankivsk (2009–2015) regions. Thus, we trained RF models independently for each region using available field observations linked to explanatory variables (Table 1) in the specified time ranges. Then we applied the models to get yearly FNF maps for 1990–2020 within each region.

2.4. GNN imputation model

We used a GEE implementation of the GNN algorithm (Ohmann & Gregory, 2002) to impute BA of individual tree species and GSV for species groups. GNN is a well-known algorithm in the family of nearest neighbors techniques that relies on canonical correspondence analysis (CCA) (ter Braak, 1986). It has been widely used across the Pacific Northwest (Bell et al., 2015, 2021; Kennedy, Ohmann, et al., 2018) and in other parts of the United States (Wilson et al., 2012) to simultaneously map distributions of various forest attributes. For the GEE implementation, we used a new library developed by the authors (GEE-KNN) which automates many of the steps in nearest neighbor techniques and allows comparative evaluation of different algorithms.

Species distribution mapping is widely used in biodiversity and conservation studies (e.g., Phalan et al., 2019). We aimed to predict the spatial patterns in 2020 of all tree species which occupy>5% of the study areas. We calculated basal area per hectare for individual species (including groups of rare species, Table 2 and Table 3) for each forested sample plot (as well as total BA), which were used to construct the CCA species matrix. For the environmental matrix, we extracted phenology-linked TCT bands, topography, and climatic data (Table 1) as inputs for GNN. As noted above and in Fig. 4, we chose not to use the harmonic coefficients as covariates in GNN as we were concerned about static CCDC coefficients being used to capture dynamic continuous vegetation patterns. We used the first eight CCA axes to identify the nearest neighbor(s) for each mapped pixel in multivariate gradient space. Given the GNN model built with the matrix of individual species BA, we aggregated predicted GSV by species groups to get more reliable estimates of volume at the pixel level. In addition, we assumed that inclusion of the species groups in the study should have more reliable application in forest management.

Given predicted values of BA for each individual species, we used a BA threshold value (1.0 $m^2\ ha^{-1}$) to create discrete presence-absence maps. Since higher values of k in GNN models tend to yield higher commission errors in such maps (Henderson et al., 2014), we used $k = 1$ to predict distributions of species, while $k > 1$ was applied to predict GSV. In addition to varying the value of k, we also tested various schemes for weighting the nearest neighbors. Given the relatively small number of observation (1196 and 838 sample plots), we finally used GNN model with $k = 3$ to get prediction of GSV for species groups. To emulate the bootstrapping approximation for weighting nearest neighbor contributions to predictions (Bell et al., 2015, 2021), we applied the following coefficients 0.7, 0.2, and 0.1 for predicting GSV attribute value.

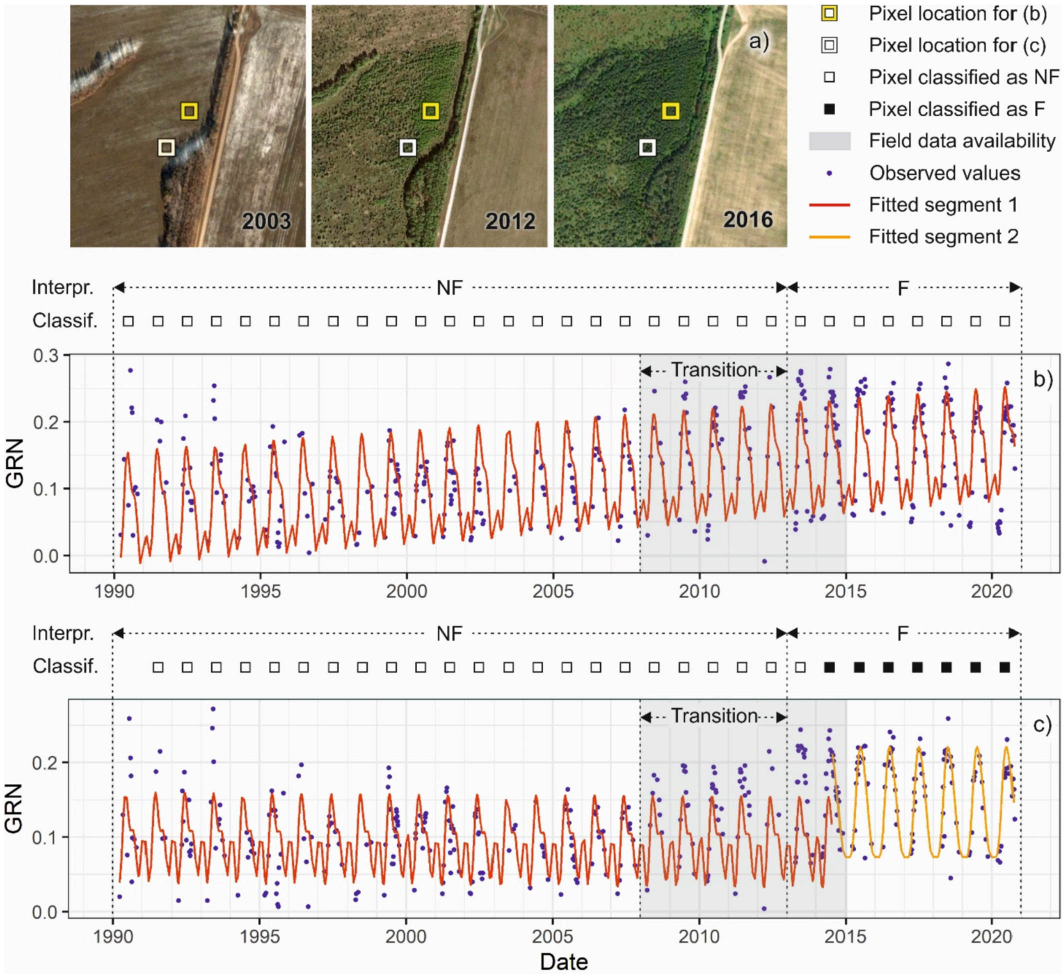

Fig. 4. An example of CCDC mapping algorithm performance within areas of forest regrowth of abandoned farmlands: (a) Google Earth images; (b) fitted time series of TCT greenness (GRN) when no forest segment detected (Lat: 52.0305, Lon: 33.7769); (c) fitted time series of GRN when forest regrowth detected with time delay (Lat: 52.0299, Lon: 33.7763); NF and F correspond to non-forest and forest, respectively. In this example, land cover is transitioning from non-forest to forest between 2008 and 2013.

Table 2
Tree species used in GNN imputation within the Ivano-Frankivsk region.

Scientific name	Code used in species mapping with $k = 1$	Species group used in GSV imputation with $k = 3$	Frequency ($n = 838$)
Picea abies L.	PIAB	CON	472
Fagus sylvatica L.	FASY	DC1	409
Abies alba L.	ABAL	CON	280
Betula pendula Roth.	BEPE	DC2	212
Quercus robur L.	QURO	DC2	168
Carpinus betulus L.	CABE	DC2	167
Acer pseudoplatanus L.	ACPS	DC1	144
Populus tremula L.	POTR	DC2	109
Tilia cordata Mill.	TICO	DC2	76
Alnus glutinosa (L.) Gaerth	ALGL	DC2	54
Pinus sylvestris L.	PISY[1]	CON	32
Other rare species of genus *Acer, Ulmus, Fraxinus, Quercus*	OTHERS	DC2	137

[1] PISY in the Ivano-Frankivsk region includes other rare coniferous species such as *Larix decidua* L. and *Pinus strobus* L.

Table 3
Tree species used in GNN imputation within the Sumy region.

Scientific name	Code used in species mapping with $k = 1$	Species group used in GSV imputation with $k = 3$	Frequency ($n = 1196$)
Quercus robur L.	QURO	QURO	580
Pinus sylvestris L.	PISY[2]	PISY	468
Acer platanoides L.	ACPL	DC1	396
Tilia cordata Mill.	TICO	DC1	372
Betula pendula Roth.	BEPE	DC2	366
Fraxinus excelsior L.	FREX	DC1	249
Populus tremula L.	POTR	DC2	153
Alnus glutinosa (L.) Gaerth	ALGL	DC2	102
Salix alba L.	SAAL	DC2	60
Other rare species of genus *Acer, Ulmus, Juglans, Carpinus, Quercus, Robinia*	OTHERS	DC1	445

[2] PISY in the Sumy region includes other rare coniferous species such as *Pinus banksiana* Lamb., *Picea abies* L., and *Larix decidua* L.

2.5. Quantifying trends of forest cover

Our approach can be used to extract forest cover information for any model year. In this study, we used 5-years intervals (i.e., 1990, 1995, …, 2020) for which we created 30-m resolution maps of forest cover, species distribution, and GSV (total and by species groups). We reported the change in forest cover for larger geographical areas as defined by the 5-km hexagonal tessellation. Information summarized across broader areas than individual pixels is often more accurate and may be more relevant for many practical applications and decision-making (Bell et al., 2018; Ohmann et al., 2014; Riemann et al., 2010). The hexagonal grid resulted in 556 and 975 5-km hexagons that seamlessly tesselate the Ivano-Frankivsk and Sumy regions, respectively. We analyzed only hexagons which were completely located within the region. We summarized proportion of total forest cover and individual species, then calculated mean GSV values (m^3 ha^{-1}) per total 5-km hexagon areas. Hexagons were attributed to a given environmental zone (see Fig. 1) by majority rule. We also mapped changes for these characteristics occurring within each hexagon in 5-year time ranges.

2.6. Model accuracy

2.6.1. RF model

The accuracy of the FNF masks was tested individually for every fifth year in a time frame of 1990–2020 (Fig. 3) using leave-one-out cross-validation. For each iteration, we fit a model using training data set (i.e., n = 3202 for Ivano-Frankivsk, and n = 9860 for Sumy) excluding the plot location for which the prediction was made in the validation data set. This procedure was repeated for each plot from the validation data set (n = 464 for Ivano-Frankivsk, and n = 769 for Sumy). Then, we followed a previously reported “good practices” assessment protocol (Olofsson et al., 2014) to estimate producer’s (PA), user’s (UA), overall (OA) accuracies, and to report on forest area dynamics with 95% confidence intervals based on validation FNF data set. For every fifth year between 1990 and 2020, we constructed a two-way error matrix of our photo-interpreted classes against the FNF map to derive class-specific area estimates (Appendix A, Table A2, Table A3). Thus, our approach not only provides an assessment of forest map accuracy through time, but also a statistically defensible estimate of forest area with associated uncertainty.

2.6.2. GNN model

For validation purposes, we used a modified version of the leave-one-out approach based on the pixel’s second nearest neighbor plot (i.e., first independent plot), which has proven efficient in numerous imputation studies from the Pacific Northwest (Henderson et al., 2019; Ohmann et al., 2014; Ohmann & Gregory, 2002). Our reference data set contains repeated measurements taken during the second forest inventory cycle, thus for each target plot, we eliminated its co-located plot and did not consider it as a candidate for the nearest neighbor. The technique used to validate GNN model differed for categorical vs. continuous variables. Although we predicted species abundance, discrete presence-absence maps were derived using BA threshold of 1.0 m^2 ha^{-1}. Since individual species distributions in our study were imputed based on GNN model with k = 1, we extracted the second nearest neighbor for each sample plot. We assessed the model skill for mapping discrete species presence maps at plot location using Cohen’s kappa coefficient (Cohen, 1960). This measure is based on the difference between the actual and chance agreement in the error matrix, and is therefore a measure of the improvement in classification accuracy compared to random classification. We also report error matrices along with associated user, producer, and overall accuracy statistics for each species (Appendix A, Table A4, Table A5).

To assess the accuracy of imputed maps based on GNN model with k = 3, the first three independent plots were used. Instead of direct evaluation of GSV maps, we assessed accuracy based on equivalent BA values. We believe such assessment is more consistent with the predictive performance of the GNN model because it is not influenced by the accuracy of the volume equations used to calculate GSV. The plot-level accuracy of the BA prediction was assessed using R-square (R^2) and root mean square error (RMSE) normalized by the observed mean values. To assess map performance at landscape-levels, we generated a polygonal layer of hexagonal tessellation with 5-km spacing between hexagon centers (~21.65 km^2) and evaluated accuracy at the hexagon-level. We followed an assessment protocol (Riemann et al., 2010) according to which hexagon-level BA values were extracted only for those pixels that co-occurred with sample plots.

The accuracy of imputed GSV changes at 5-km hexagon level was evaluated as specified above using equivalent BA values and assessment protocol suggested by Riemann et al. (2010) for only those plot locations where repeated field measurements were available, i.e., 252 plot locations in the Ivano-Frankivsk region and 403 plot locations in the Sumy region.

3. Results

3.1. Dynamics of forested area

Accuracies of the FNF maps were consistent across time for both regions. The RF model exhibited good performance in terms of low commission and omission errors over the reported time period (Table 4; Appendix A, Table A2, Table A3). The accuracies were high within our regions and stable in time (OA > 0.96 ± 0.02; UA > 0.94 ± 0.03; PA > 0.93 ± 0.04). Slightly different regional performance of the model may be due to the spatial pattern of the forests. The Ivano-Frankivsk region has a greater level of forest cover (about 40%), is less fragmented, and those forests are primarily located in the Carpathian Mountains. The forests in the Sumy region are heavily fragmented, occupy a minority of the total area (~20%), and are distributed in a discontinuous manner.

Over the 30-year time period, we observed increasing trends in total forested area in both regions (Table 4, Appendix A, Fig. A1). Based on LTS classification, the total forested area in the Ivano-Frankivsk region increased from 599.4 ± 23.0 ha in 1990 to 627.3 ± 23.6 ha in 2020. The rates of forest gain here were greatest during 1995–2000 due to forest regrowth on previously harvested areas, followed by relatively little change in forest cover across the region over the following 20 years. The forested area in the Sumy region experienced a steady increase from 429.0 ± 23.9 ha in 1990 to 512.5 ± 27.0 ha in 2020. During the last three decades, we observed an increase in the forested proportion of the region from 0.180 to 0.215, representing a 19% increase in forested area.

Expressing forests in terms of proportion of forest cover within 5-km hexagons allowed us to derive more details from forest spatial distribution (e.g., contiguity, patchiness, etc.). The forest maps in 2020 expressed as proportion of the total hexagon area (Fig. 5) indicate different spatial patterns of forest distribution within our regions. The Carpathian Mountains (western portion of Ivano-Frankivsk) were generally characterized by forests area with>75% of the hexagon area. In contrast, one can notice only a few locations in the Sumy region representing such level of forested area.

We also used this hexagonal tessellation to analyze the spatio-temporal pattern of forest cover change for longer time periods. We applied 10-year intervals to highlight hexagons within which major changes were observed (Fig. 6). The forest loss in the Ivano-Frankivsk region varied between 1% and 6% during 1990–2000, and ranged from 1% to 10% during 2010–2020. Forest gain was a prominent feature of forest change in the Sumy region where forested area tended to increase in the Polissia zone from 1% to 8% in 1990–2000 up to 1%–13% in 2010–2020. The rates of forest change during 2000–2010 for both regions were interim within specified tendencies, apart from one hexagon on Fig. 6b for which we estimated 14% of forest loss due to the development of the infrastructure in Bukovel ski resort village. Our FNF maps enable extraction of more detailed spatial and temporal patterns of forest change that provide valuable insight into forest management (Appendix A, Fig. A2).

Table 4
Regional estimates of forest cover dynamics (at 95% confidence level).

Year	Forested area, thousands ha		Estimated area proportion	User's accuracy	Producer's accuracy	Overall accuracy
	mapped	estimated				
Ivano-Frankivsk region						
1990	603.9	599.4 ± 23.0	0.430 ± 0.017	0.957 ± 0.028	0.964 ± 0.025	0.966 ± 0.017
1995	607.5	605.0 ± 25.1	0.434 ± 0.018	0.951 ± 0.030	0.955 ± 0.028	0.959 ± 0.018
2000	613.4	611.9 ± 23.8	0.439 ± 0.017	0.958 ± 0.027	0.959 ± 0.027	0.964 ± 0.017
2005	621.2	623.1 ± 24.5	0.447 ± 0.018	0.958 ± 0.027	0.955 ± 0.027	0.961 ± 0.018
2010	625.7	630.0 ± 23.9	0.452 ± 0.017	0.963 ± 0.025	0.956 ± 0.027	0.963 ± 0.017
2015	634.5	628.7 ± 22.3	0.451 ± 0.016	0.960 ± 0.026	0.970 ± 0.023	0.968 ± 0.016
2020	633.5	627.3 ± 23.6	0.450 ± 0.017	0.955 ± 0.027	0.965 ± 0.025	0.964 ± 0.017
Sumy region						
1990	423.4	429.9 ± 23.9	0.180 ± 0.010	0.948 ± 0.035	0.933 ± 0.040	0.979 ± 0.010
1995	437.8	435.0 ± 22.9	0.183 ± 0.010	0.943 ± 0.036	0.949 ± 0.036	0.980 ± 0.010
2000	454.4	457.3 ± 23.2	0.192 ± 0.010	0.951 ± 0.033	0.944 ± 0.036	0.980 ± 0.010
2005	468.5	471.5 ± 24.7	0.198 ± 0.010	0.945 ± 0.035	0.939 ± 0.037	0.977 ± 0.010
2010	482.5	485.9 ± 24.6	0.204 ± 0.010	0.948 ± 0.033	0.941 ± 0.036	0.977 ± 0.010
2015	503.3	513.6 ± 24.7	0.215 ± 0.010	0.957 ± 0.030	0.937 ± 0.036	0.977 ± 0.010
2020	507.3	512.5 ± 27.0	0.215 ± 0.011	0.941 ± 0.034	0.931 ± 0.038	0.973 ± 0.011

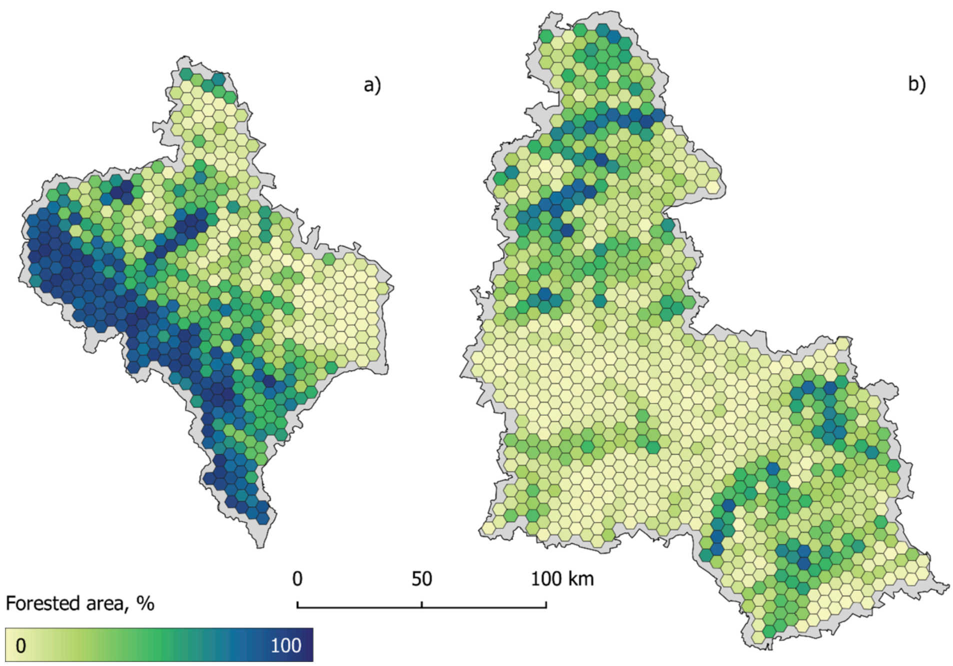

Fig. 5. Forested area expressed as proportion of forest area mapped using LTS for 2020 and total area of 5 km hexagon: (a) Ivano-Frankivsk region, (b) Sumy region.

3.2. Species distribution and abundance

The skill (Cohen's kappa) of presence-absence maps tended to increase and overall accuracy tended to decrease with species prevalence across the study region (Table 5). Overall accuracy varied from 65% to 94%, with eight species exhibiting accuracy>85%, with a tendency toward decreasing accuracy with decreasing prevalence in both Ivano-Frankivsk (Pearson correlation = -0.65) and Sumy (Pearson correlation = -0.70) regions. In both regions, GNN predictions of *Pinus sylvestris* and *Alnus glutinosa* presence and absence exhibited consistently high accuracy (>85%). User's and producer's accuracies were highly correlated (Pearson correlation > 0.99), indicating similar tendencies for omission as commission. The skill of GNN models increased with mean BA and species prevalence, summarized at the 20-km hexagon-level to include a sufficient number of plots (Fig. 7, Fig. 8). Our model exhibited greater skill for *Picea abies* in the Ivano-Frankivsk (Cohen's kappa = 0.500) and *Pinus sylvestris* in the Sumy region (Cohen's kappa = 0.800) that had relatively higher mean values of BA (Appendix A, Table A6), and often grew in pure stands. In contrast, GNN predictions for some rare species was not much better than random prediction (e.g., *Acer pseudoplatanus*, Cohen's kappa = 0.081). Deciduous species, which normally grow in mixed stands (e.g., *Fraxinus excelsior*, *Acer platanoides*, and *Tilia cordata* in the Sumy region), tended to exhibit similar map skill. Predictive performance of GNN for species distributions was not obviously associated with their proximity to mountains, flat land areas, or other specific different environmental zones.

The mapped distributions of the six most common species (prevalence ≥ 20%) for both study regions were similar to the observed spatial patterns using sample plots data at landscape-scales, represented here by 20-km hexagons (Fig. 7, Fig. 8). We found a strong relationship (in general, correlation coefficient > 0.8) between the number of sample plots where the species is observed (BA > 1.0 m^2 ha^{-1}) and its mapped area within 20-km hexagons. Interestingly, our analysis showed different levels of agreement for *Betula pendula* in the Ivano-Frankivsk and Sumy regions, for which we observed differences in the absolute values of BA (mean: 1.2 vs. 2.1 m^2 ha^{-1}; 97.5th percentile: 11.0 vs. 20.0 m^2 ha^{-1}) at plot locations (Appendix A, Table A6).

Predictive mapping of BA for plant communities representing certain

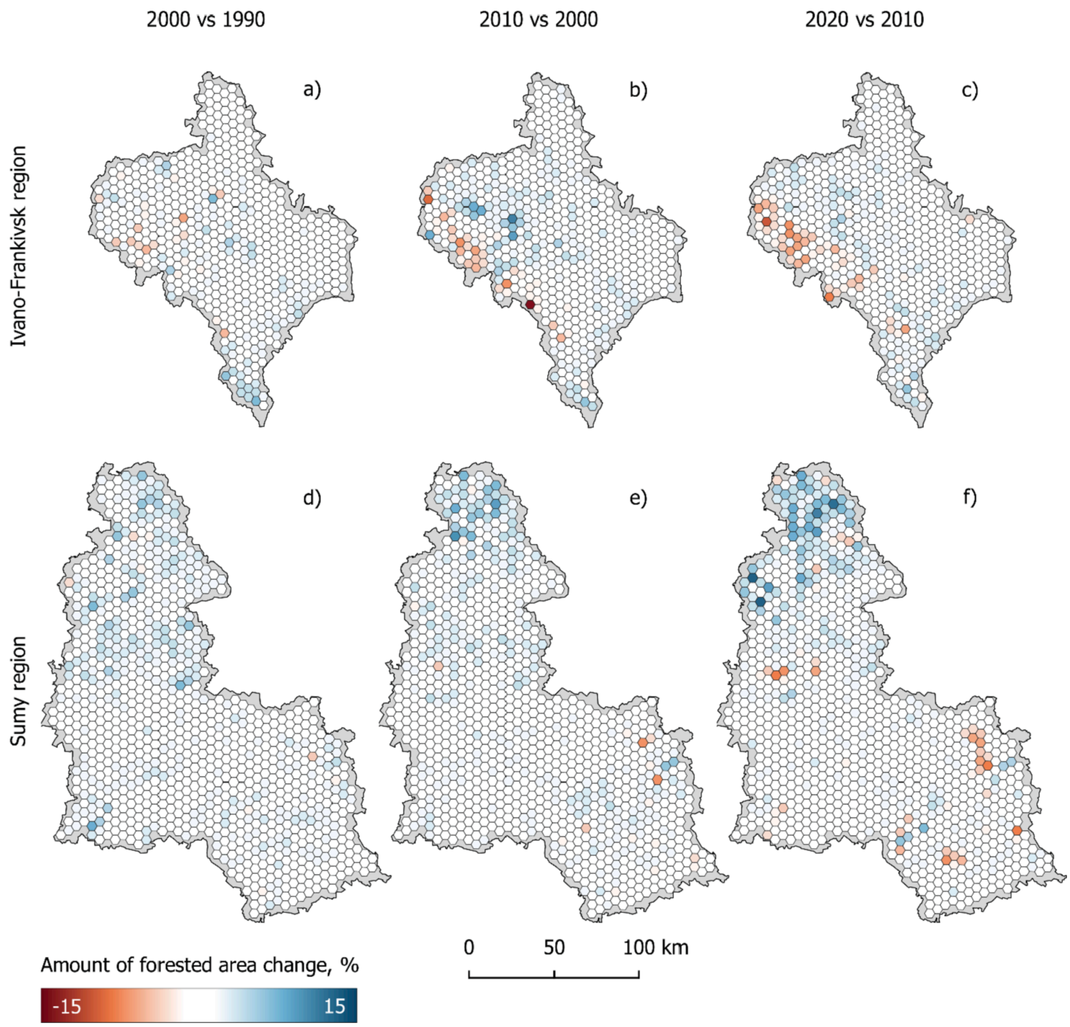

Fig. 6. Spatial pattern of forested area change within 5 km hexagons for Ivano-Frankivsk (a), (b), (c) and Sumy (d), (e), (f) regions: (a), (d) 2000 vs 1990; (b), (e) 2010 vs 2000; (c), (f) 2020 vs 2010.

Table 5
Regional accuracy of tree species mapping based on GNN imputation model ($k = 1$).

Species	Prevalence	Cohen's kappa	Overall Acc. (%)	Species	Prevalence	Cohen's kappa	Overall Acc. (%)
Ivano-Frankivsk region							
PIAB	0.563	0.500	75.3	ACPS	0.172	0.081	73.3
FASY	0.488	0.439	72.0	POTR	0.130	0.097	79.7
ABAL	0.334	0.328	69.8	TICO	0.091	0.211	86.8
BEPE	0.253	0.197	69.5	ALGL	0.064	0.166	89.9
QURO	0.200	0.536	85.1	PISY	0.038	0.159	93.9
CABE	0.199	0.562	85.4	OTHERS	0.163	0.118	74.8
Sumy region							
QURO	0.485	0.355	67.7	FREX	0.207	0.431	81.4
PISY	0.391	0.800	90.5	POTR	0.128	0.127	81.0
ACPL	0.331	0.466	76.1	ALGL	0.085	0.441	91.6
TICO	0.311	0.390	73.7	SAAL	0.050	0.309	93.6
BEPE	0.306	0.346	72.4	OTHERS	0.372	0.254	64.7

ecological niches was better than for individual species (Table 6). Similar to species distribution, performance of the species abundance models was strongly associated with mean value of BA. For example, the R^2 values at plot locations ranged from poor (less than 0.0) to better (0.1–0.3) for less abundant species (Appendix A, Table A6), while we attained better accuracy ($R^2 > 0.3$) for the majority of species groups (Table 6). By aggregating tree species into relatively broad groups, we observed better correspondence between hexagon observed and predicted mean values of BA for individual species and species groups (Table 6). When this correspondence is observed on scatterplots, it means a stronger association of paired observed and predicted values along the 1:1 identity line (Appendix A, Fig. A3, Fig. A4).

3.3. *Mapping growing stock volume*

The total GSV maps were imputed using $k = 3$ at 30-m spatial resolution. Fig. 9 depicts a major difference in spatial pattern of forest cover and associated GSV between mountain and flat land Ukraine. We found

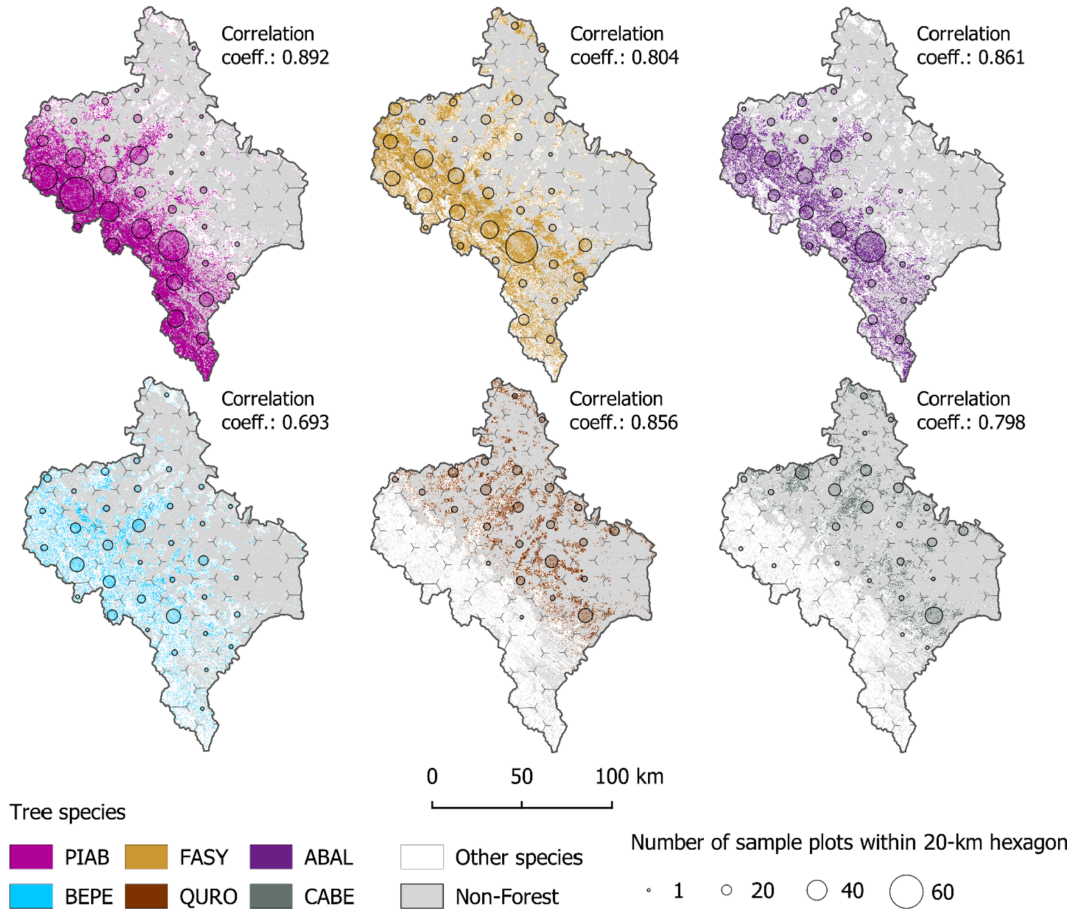

Fig. 7. Distribution of individual species within the Ivano-Frankivsk region based on GNN imputation (k = 1): correlation coefficients represent the relationship between mapped area of species within 20-km hexagon and number of sample plots where it is observed.

that total GSV of mountain forest at pixel level was substantially higher and reached values up to 1300 m^3 ha^{-1} (Fig. 9a), whereas the maximum pixel values of the total GSV in flat land areas of the Sumy and Ivano-Frankivsk regions reached only 750 m^3 ha^{-1}.

Scatterplots of observed and predicted values of BA change showed fair agreement with 1:1 identity line only when data were aggregated at hexagonal level (Appendix A, Fig. A5). Consequently, the GSV change metrics were derived using 5-km hexagonal tessellation for 10-year intervals between 1990 and 2020 (Fig. 10). These spatially explicit products allowed us to explore GSV distribution over the study regions for the last three decades. Dynamics of the total GSV for both our study regions had similar tendencies. We observed faster forest growth in 1990–2000 which was characterized by an annual increment of the GSV at hexagon level up to 10 m^3 ha^{-1} yearly. Since this value was calculated using total hexagon area, one should expect higher values if forest cover within 5-km hexagon was lower than 100%. Since the most evident trends of positive GSV dynamics were associated with highly forested areas, forests in 1990–2000 appear to be systematically younger and experienced greater rates of GSV increment. Starting from 2000 to 2010, the loss of total GSV increased in 2010–2020 approaching values of −7 m^3 ha^{-1} yearly. We detected distinct locations of dramatic GSV loss that we can associate with intensified harvesting during the last decade (Fig. 10c, Fig. 10f). The dynamics of forested area (Fig. 6) and GSV (Fig. 10) demonstrate good agreement. The hexagons with loss of total GSV are synchronized with the decrease of the forested area proportion. This was not always necessarily the case in the northern part of the Sumy region, where a decrease of the GSV due to harvesting was very often hidden by intensive afforestation within 5-km hexagons.

4. Discussion

In this study, we sought to gain a more comprehensive understanding of the main trends in forest change derived from using an independent source of information and deliver this information to forest management of Ukraine. Although>99% of forests are state-owned in Ukraine, information about forest change has not been systematically updated by different agencies. Our research is the first attempt to produce a spatially-explicit, multidecadal (1990–2020) assessment of forested area, GSV change, and species distributions within two different regions of Ukraine. Similar ideas have already been discussed in previous studies for other geographic regions such as Australia by Nguyen et al. (2020), however, a key novelty of this research lies in the integration of the CCDC segmentation approach, RF classification algorithm, and nearest neighbor imputation technique into a single workflow to uncover spatio-temporal dynamics of the forested areas using the GEE cloud-based platform. As described below, the multi-decadal trends in forested area and growing stock volume documented in this study reflect spatial and compositional differences in the effects of historical forest management and changing land use since the fall of the Soviet Union. Our results highlight the importance of fostering methodological advances in the national forest inventory in Ukraine.

4.1. Forested area and GSV change

This paper emphasizes the utility of leveraging LTS in a cloud computing environment to extend even sparse, temporally short forest inventories over a limited time frames to provide long-term forest monitoring. Though some nations, such as the United States and

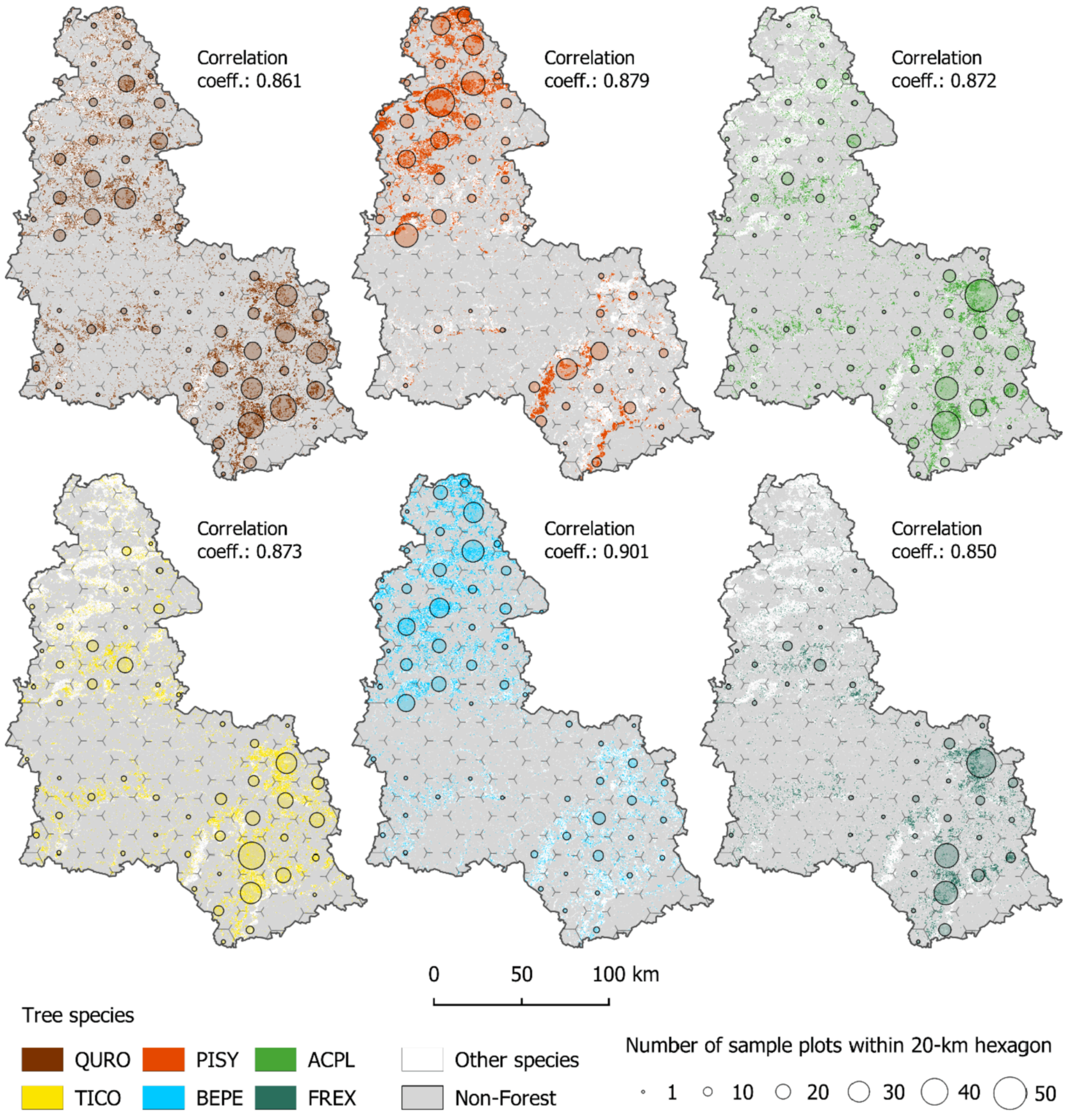

Fig. 8. Distribution of individual species within the Sumy region based on GNN imputation (k = 1): correlation coefficients represent the relationship between mapped area of species within 20-km hexagon and number of sample plots where it is observed.

Table 6
Prediction accuracy of the GNN imputation model (k = 3) at plot and 5-km hexagon levels by species groups.

Species group	Observed BA's mean, $m^2 ha^{-1}$	Predicted BA's mean, $m^2 ha^{-1}$	Plot locations		5-km hexagon locations	
			Normalized RMSE	R^2	Normalized RMSE	R^2
Ivano-Frankivsk region						
CON	16.1	16.0	0.779	0.531	0.478	0.741
DC1	9.0	9.6	1.25	0.333	0.778	0.574
DC2	6.6	7.0	1.19	0.353	0.831	0.592
Total BA	31.8	32.6	0.456	0.235	0.294	0.502
Sumy region						
QURO	5.2	5.8	1.33	0.274	0.894	0.487
PISY	9.0	9.2	0.817	0.712	0.540	0.825
DC1	7.1	7.1	1.04	0.416	0.716	0.623
DC2	4.6	4.7	1.66	0.129	1.10	0.360
Total BA	26.0	26.8	0.410	0.157	0.279	0.214

Norway, have long-term, field-based, extensive, and consistent design-based forest inventories (Breidenbach et al., 2020), many nations do not have the resources to sustain such efforts, particularly for nations with large and remote forest regions. For example, the sample plot data for the Sumy and Ivano-Frankivsk regions of Ukraine were restricted in temporal domain to 2008–2015. By integrating these data with the Landsat satellite image archive, we used these plots to characterize three decades of forest cover dynamics, an effort not possible based solely on the seven years of forest inventory data.

The forested area in our study regions was not stable over time. In the

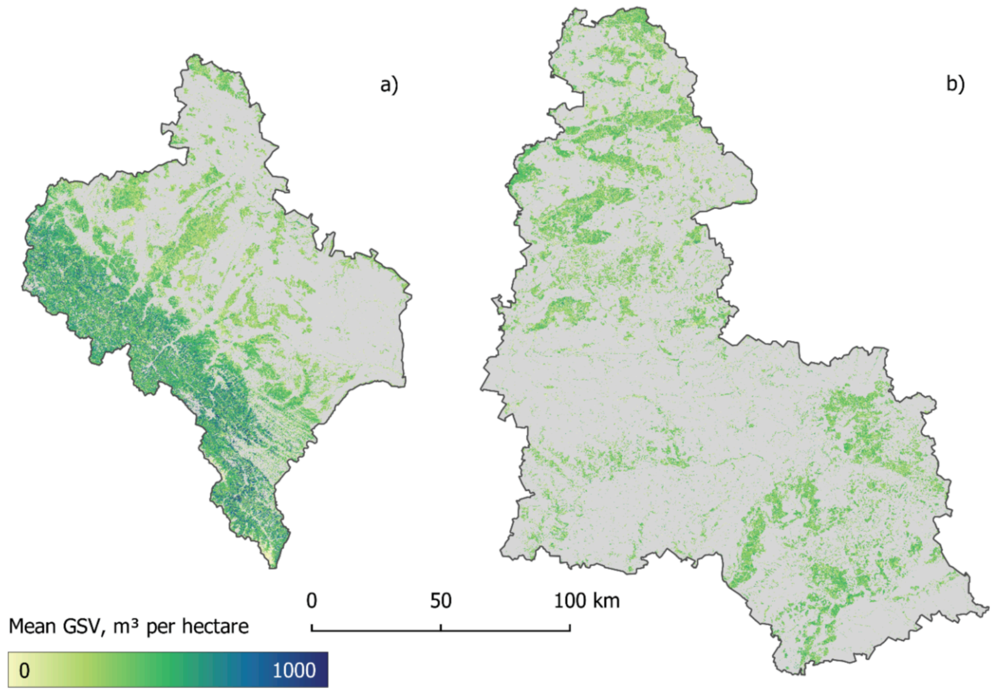

Fig. 9. Mean total GSV imputed for 2020 using the GNN model (k = 3): a) Ivano-Frankivsk region; b) Sumy region.

Ivano-Frankivsk region, we documented two waves of forest cover loss in the mountain area between 2000 and 2010 and 2010–2020 (Fig. 6). For example, some 5-km hexagons experienced>5% forest area loss over some five-year intervals. This finding supports published results for the region (Oliinyk, 2019) that documented an increase of the total area under all kinds of timber harvesting (clear cutting, thinning, salvage logging) from about 20,000 ha in 2005 to almost 30,000 ha in 2015.

The Sumy region exhibited another interesting trend in forest dynamics that is also worth discussion. As with previous studies focused on Polissia zone of Ukraine (Stefanski et al., 2014), we detected two periods of farmland abandonment with higher afforestation rates. The first one was characterized by a period of forest regrowth during 1990–2000, which coincided with the breakdown of the Soviet Union in 1991. There was a dramatic shift in land management, leading to the abandonment of large agricultural lands throughout Ukraine. Cumulative farmland abandonment in the Polissia zone intensified during 2000–2010 after the land reforms that led to disbanding of collective farms (kolkhoz – a left-over of Soviet economic system). Thus, we detected more areas with forest gain in 2010–2020 when former kolkhozs' farmlands were regrown into forests (Fig. 6).

Forest maps produced in this study represent a temporally consistent regional characterization of forest cover for the period of 1990–2020 at a spatial resolution of 30 m that meets the requirements of forest monitoring programs. In particular, our results are consistent with previous estimates of forested areas in the Sumy region circa 2014–2016 (Myroniuk et al., 2020), although with this study we have improved both user's and producer's accuracy by about 3%. Through within-region environmental zone analysis, important differences emerged in the performance of the RF classification model. In our case, we observed that the accuracy of forest maps appeared to be a function of the spatial pattern of forests: greater fragmentation of forest landscapes was associated with less precise and less accurate estimates of forested area. For example, higher accuracies for the Ivano-Frankivsk region may be due to the fact that>70% of its forested area was represented by the contiguous forests in the mountains. Accuracy was correspondingly lower for the Sumy region where there are severely fragmented forest landscapes. Given the different spatial patterns of the forest cover even within a region, we would suggest developing separate classification models for certain environmental zones to map forests at the national level in Ukraine. Such a strategy allows high accuracy FNF maps for most forested regions and if necessary, fine-tuning the mapping approach for areas with more fragmented forests.

Growing stock volume is a key characteristic of forests and is widely used to support forest management in Ukraine, such as to regulate annual allowable cuts. Spatial and temporal GSV dynamics showed that losses were associated with relevant forested area change. During the last two decades, we discovered increased rates of GSV loss in the Carpathian Mountains (Fig. 10) due to wood harvesting. Unfortunately, there is no independent spatially explicit information about the temporal dynamics of forests in Ukraine, but our predicted forest loss maps in the last decades corroborate previously reported intensification of logging activities in the Carpathians region from 0.9 million m^3 of total wood volume in 2005 to 1.5 million m^3 in 2015 (Oliinyk, 2019).

This study showed explicit trends of forest change which were affected by health and age structure of forests. Logging in the Carpathian Mountains was most intensive after the Second World War. The timber volume harvested in mature forests (>80 years) was up to three times higher than it was scientifically recommended given the current structure of forests. By way of explanation, 3.67, 3.26 and 2.22 million m^3 were harvested in the Ivano-Frankivsk region in 1950, 1955 and 1960, respectively (Holubchak et al., 2018). Similar patterns of forest harvest were quantified using historical CORONA spy satellite photography within the bordering Carpathian Mountains in Romania when its economy was recovering after the Second World War (Nita et al., 2018). Thus, large areas of forests that were planted in 1950 s and 1960 s appeared to achieve increased growth rates during 1990–2000 (Fig. 10). Conversely, salvage logging in spruce stands in the Ivano-Frankivsk region, and in pine forest in the Sumy region, may have substantially contributed to forest area losses during the last decade (Fig. 6).

4.2. CCDC integration into regional monitoring and mapping

Our research highlights the value of leveraging both the inter- and intra-annual variation in satellite imagery provided by the CCDC algorithm as a foundation for regional, multidecadal forest monitoring. We have highlighted major aspects of regional forest mapping along

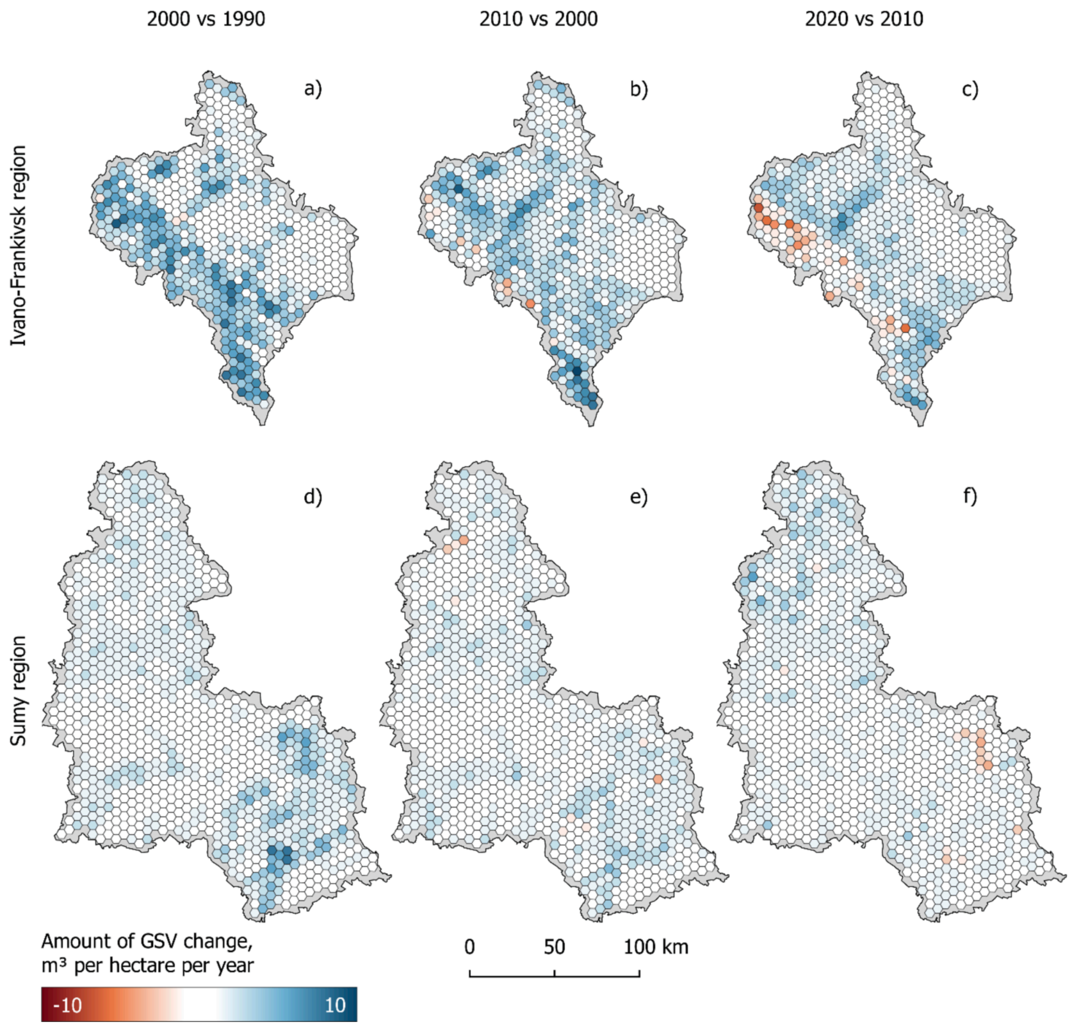

Fig. 10. Spatial pattern of GSV change within 5-km hexagons for Ivano-Frankivsk (a), (b), (c) and Sumy (d), (e), (f) regions: (a), (d) 2000 vs 1990; (b), (e) 2010 vs 2000; (c), (f) 2020 vs 2010.

gradients of environmental factors and various spatial patterns of forest cover in Ukraine. The harmonic coefficients from the original CCDC approach (Zhu & Woodcock, 2014) showed good performance in mapping stable land cover classes and rapid forest loss events, but similarly to (Brown et al., 2020) did not necessarily capture gradual afforestation processes on former agricultural fields (e.g., Fig. 4). However, spectral information derived from CCDC harmonic regression allowed us to depict gradual and long-lasting forest recovery more precisely. One of the most significant benefits from the combination of spectral data, coefficients, and derivatives of the CCDC approach was in producing temporally consistent FNF classification for the same pixel to get precise estimates of forested area dynamics in 1990–2020 (Table 4; Appendix A, Fig. A1, Table A2, Table A3).

We showed that the nearest neighbor imputation technique in combination with the CCDC segmentation is a powerful approach to uncovering multiyear trends of forest attribute change. Separate models were developed for the Ivano-Frankivsk and Sumy regions to predominantly constrain the nearest neighbor imputation of species data to reasonable locations (i.e., roughly to the environmental zones) where structural attributes dominate the ordination. This is perhaps the first example of the application of the CCDC approach in conjunction with nearest neighbor imputation of continuous forest attributes. Our approach used the first three components of TCT that were phenologically linked to the start, middle, and end of the leaf-on period, though we are aware that the optimal set of spectral variables might be linked to other dates in other landscapes. From this point of view, the CCDC harmonic regression algorithm provides outstanding opportunities to extract the best seasonal information from LTS. An interesting methodological aspect of mapping forest attribute dynamics could be testing nearest neighbor imputation approaches based on synthetic values of spectral bands for different dates versus the CCDC coefficients. As demonstrated in Fig. 4, areas which undergo subtle changes over time may only have a single harmonic segment (i.e., identical CCDC coefficients), but potentially large differences in fitted synthetic values. This issue merits consideration if plot data is available for a long time range in order to capture these differences in covariate values. Unfortunately, our study did not have the temporal range to test this methodology.

4.3. Management implications

From a management perspective, this study supports a diverse range of applications. In addition to introducing the national forest inventory of Ukraine as a foundation for spatially explicit mapping of forest attributes, we gained valuable insights into their dynamics. Specifically, monitoring forest logging or infrastructure development (Appendix A, Fig. A2) in the Carpathians Mountains is important to identifying tradeoffs between ecosystem services such as erosion protection, flood regulations, recreations, and wood supply. Detected hotspots with significant forest losses (Fig. 6, Fig. 10) highlight the importance of balancing various services and promoting multifunctional forest management strategies in the Ivano-Frankivsk region. In this context, our mapping supports optimization of the spatial distribution of wood harvesting and its intensity along with conservation of old-grown forests in the future. Since flood frequency is negatively correlated with the amount of remaining natural forest and positively correlated with forest loss (Bradshaw et al., 2007), forest management may aim to ensure a balance between wood harvesting and ecosystem services related to water stock regulation. We present to forest managers valuable inputs for prioritizing forest restoration projects (yearly maps of forest loss) and planting relatively balanced mixed forest stands (maps of species distribution) that contribute most to fulfillment of targeting synergy of ecosystem services as it was widely implemented in many European countries (Orsi et al., 2020).

As a contribution to the new European Union Forest Strategy, the Government of Ukraine in 2021 approved the Environmental Security and Climate Adaptation Strategy until 2030 (*Executive Order No. 1363-p*). Ukraine is expected to increase national forest area in the next 10 years by 2% (from officially recognized 15.9% to 18%) through afforestation of low productive and degraded lands and preservation of natural forest regrowth, indicating a need for reliable information about the status and trends in forest extent, such as those provided by our mapping efforts. While many farmlands have been abandoned since the early 1990s north of Ukraine and turned into forests, these areas could significantly contribute to the total area of forests, though those areas of afforestation may still account for a small component of regional carbon sequestration if their growth is not similar to extant forests. We provided a regional-level mapping approach to detect forest regrowth (Appendix A, Fig. A2), though a thoughtful land policy required to minimize the risks of clearing such areas from trees by private owners or farmers. In contrast to well-known products of forest change detections (Hansen et al., 2013), the nearest neighbor imputation algorithm provides a more comprehensive estimation of forest characteristics that can be used in the calculation of ecosystem services (e.g., carbon sequestration) for such areas. For example, GSV is a key parameter for assessing live biomass (Bilous et al., 2017) and carbon stock of forest ecosystems in Ukraine (Lakyda et al., 2019). From this perspective, imputed maps of GSV dynamics can be used to support decision making related to the achievement of carbon neutrality at regional level. The framework we have introduced, especially using our cloud-computing based workflow, could be easily extended to support national-level estimates with the introduction of more forest inventory plots.

4.4. Potential limitations to multidecadal mapping

Early examination of multispectral data and subsequent FNF mapping indicated low magnitude, multi-decadal shifts in several multispectral indices. Multidecadal shifts in spectral indices have been noted elsewhere, such as those observed for Landsat 5 as gradual changes in orbital path caused erroneous detections of vegetation “browning” and underestimations of “greening” (Roy et al., 2016). In our study, initial evaluation of forest mapping using the plot data collected during 2008–2015 and the LTS indicated that these shifts might result in substantial omission of forest prior to 2000 and commission in 2020. Based on high-resolution images interpretation, such changes were often associated with stable forest. To address this challenge, we used a combination of fitted imagery and harmonic regression coefficients from CCDC to capture inter- and intra-annual vegetation dynamics relevant to forest mapping. Visual inspection of the resulting FNF maps and historical satellite images indicate that our approach minimized omission and commission errors over the study period (1990–2020). Our results support the use of not only spectral harmonization, but also inter-annual and seasonal trend analyses through algorithms like CCDC.

As opposed to the FNF mapping, where we could generate historical (1990–2020) training and validation data through images interpretation, GNN relied only on the field-based inventory (2008–2015). As a result, we extrapolated beyond the temporal domain of our field data, assuming that the relationships between predictor and response variables were stationary through time (*sensu* Ohmann et al., 2012, Davis et al., 2015, Kennedy et al., 2018). Multidecadal shifts in spectral indices described above may be explained by, among other things, orbital drift for Landsat 5 decreasing NDVI (Roy et al., 2016) or increasing exposure of non-leaf material, such as lichen and bark (Cohen & Spies, 1992). Such changes can have dramatic impacts on imputation, motivating additional measures to minimize errors. For example, mapping old-growth forest (200–500 years old) in the Pacific Northwest USA, long-term increasing TCT brightness in otherwise stable, old forests led to predictions of forests growing younger through time, which seems unreasonable (Davis et al. in press). This result led to the use of long-term mean spectral data in older forests with no disturbance identified or censoring out predicted old-growth forest pixels that were also observed to experience disturbance in earlier years (Davis et al., in press, Bell et al., 2021). That stabilization recognizes that undisturbed forests may vary spatially in terms of structure and composition, but that the Landsat imagery lacks much information regarding changes in forest structure over just a few decades in these older forests. While we have not modified our spectral covariates for this study, areas of subtle change over decades of Landsat imagery may be susceptible to similar issues stemming from using imputation techniques.

5. Conclusions

Demand for high-quality, spatially and temporally detailed forest information is increasing in various applications. In this research, we demonstrated the opportunities for extending applications of temporally limited historical forest inventory data using LTS and a cloud computing environment to support research and forest management at regional level. From a methodological perspective, we have introduced a nearest neighbor imputation workflow in the GEE cloud-based platform, enabling other users with similar plot inventories to follow this methodology. We evaluated predictive performance of RF classification and GNN imputation techniques that utilized all available historical forest inventory data linked with the temporally normalized LTS. We found that fitted inter- and intra-annual trends in LTS extracted using the CCDC segmentation algorithm strengthened multidecadal assessment of forest characteristics. Application of harmonic model coefficients and synthetic images created with the CCDC algorithm allowed us to uncover forest area dynamics at 5-year intervals across the temporal domain. Still, we believe that inter- and intra-annual variation of spectral indices is more reliable to depict dynamic of continuous forest attributes (BA, GSV). Although our accuracy was good for the most practical applications, our understanding of the applicability of the nearest neighbor imputation approach was restricted to the time range of field data collection. New field information collected during forthcoming forest inventory cycles in Ukraine that has resumed in 2021 will enable further evaluation of the forecasting strategy of forest attribute mapping presented in this study.

CRediT authorship contribution statement

Viktor Myroniuk: Conceptualization, Funding acquisition, Methodology, Data curation, Formal analysis, Software, Validation, Visualization, Writing – original draft, Writing – review & editing. **David M. Bell:** Conceptualization, Methodology, Formal analysis, Resources, Writing – original draft, Writing – review & editing. **Matthew J. Gregory:** Methodology, Resources, Software, Formal analysis, Data curation, Writing – original draft, Writing – review & editing. **Roman Vasylyshyn:** Resources, Investigation. **Andrii Bilous:** Resources, Investigation.

Declaration of Competing Interest

The authors declare that they have no known competing financial interests or personal relationships that could have appeared to influence the work reported in this paper.

Acknowledgements

This research was funded by the U.S. Department of Agriculture Forest Service Pacific Northwest Research station and the Fulbright Program sponsored by the U.S. Department of State, Bureau of Educational and Cultural Affairs (ECA), Exchange Visitor Program #G-1-00005, under Project "Tracking Forest Fragmentation in Ukraine and the Western United States: A Comparative Analysis Based on Remote Sensing Approach and Management Implication" (Program number G-1-00005; IIE ID: PS00302916). We would like to acknowledge the role of the Center of the National Forest Inventory of Ukraine in field data collection. We also would like to thank V. Storozhuk for providing forest inventory data. We are also thankful to two anonymous reviewers for their very helpful and constructive comments.

Appendix A. Supplementary data

Supplementary data to this article can be found online at https://doi.org/10.1016/j.foreco.2022.120184.

References

Abatzoglou, J.T., Dobrowski, S.Z., Parks, S.A., Hegewisch, K.C., 2018. TerraClimate, a high-resolution global dataset of monthly climate and climatic water balance from 1958–2015. Sci. Data 5 (1), 170191. https://doi.org/10.1038/sdata.2017.191.

Adams, B., Iverson, L., Matthews, S., Peters, M., Prasad, A., Hix, D.M., 2020. Mapping Forest Composition with Landsat Time Series: An Evaluation of Seasonal Composites and Harmonic Regression. Remote Sensing 12 (4), 610. https://doi.org/10.3390/rs12040610.

Arévalo, P., Bullock, E.L., Woodcock, C.E., Olofsson, P., 2020. A Suite of Tools for Continuous Land Change Monitoring in Google Earth Engine. Frontiers in Climate 2, 576740. https://doi.org/10.3389/fclim.2020.576740.

Awty-Carroll, K., Bunting, P., Hardy, A., Bell, G., 2019. An Evaluation and Comparison of Four Dense Time Series Change Detection Methods Using Simulated Data. Remote Sensing 11 (23), 2779. https://doi.org/10.3390/rs11232779.

Banskota, A., Kayastha, N., Falkowski, M.J., Wulder, M.A., Froese, R.E., White, J.C., 2014. Forest Monitoring Using Landsat Time Series Data: A Review. Canadian Journal of Remote Sensing 40 (5), 362–384. https://doi.org/10.1080/07038992.2014.987376.

Beaudoin, A., Bernier, P.Y., Villemaire, P., Guindon, L., Guo, X.J., 2018. Tracking forest attributes across Canada between 2001 and 2011 using a *k* nearest neighbors mapping approach applied to MODIS imagery. Can. J. For. Res. 48 (1), 85–93. https://doi.org/10.1139/cjfr-2017-0184.

Bell, D.M., Acker, S.A., Gregory, M.J., Davis, R.J., Garcia, B.A., 2021. Quantifying regional trends in large live tree and snag availability in support of forest management. For. Ecol. Manage. 479, 118554 https://doi.org/10.1016/j.foreco.2020.118554.

Bell, D.M., Gregory, M.J., Kane, V., Kane, J., Kennedy, R.E., Roberts, H.M., Yang, Z., 2018. Multiscale divergence between Landsat- and lidar-based biomass mapping is related to regional variation in canopy cover and composition. Carbon Balance Manage. 13 (1), 15. https://doi.org/10.1186/s13021-018-0104-6.

Bell, D.M., Gregory, M.J., Ohmann, J.L., 2015. Imputed forest structure uncertainty varies across elevational and longitudinal gradients in the western Cascade Mountains, Oregon, USA. For. Ecol. Manage. 358, 154–164. https://doi.org/10.1016/j.foreco.2015.09.007.

Bey, A., Sánchez-Paus Díaz, A., Maniatis, D., Marchi, G., Mollicone, D., Ricci, S., Bastin, J.-F., Moore, R., Federici, S., Rezende, M., Patriarca, C., Turia, R., Gamoga, G., Abe, H., Kaidong, E., Miceli, G., 2016. Collect Earth: Land Use and Land Cover Assessment through Augmented Visual Interpretation. Remote Sensing 8 (10), 807. https://doi.org/10.3390/rs8100807.

Bilous, A., Myroniuk, V., Holiaka, D., Bilous, S., See, L., Schepaschenko, D., 2017. Mapping growing stock volume and forest live biomass: A case study of the Polissya region of Ukraine. Environ. Res. Lett. 12 (10), 13. https://doi.org/10.1088/1748-9326/aa8352.

Bolton, D.K., Coops, N.C., Hermosilla, T., Wulder, M.A., White, J.C., Ferster, C.J., 2019. Uncovering regional variability in disturbance trends between parks and greater park ecosystems across Canada (1985–2015). Sci. Rep. 9 (1), 1323. https://doi.org/10.1038/s41598-018-37265-4.

Bradshaw, C.J.A., Sodhi, N.S., Peh, K.-S.-H., Brook, B.W., 2007. Global evidence that deforestation amplifies flood risk and severity in the developing world. Glob. Change Biol. 13 (11), 2379–2395. https://doi.org/10.1111/j.1365-2486.2007.01446.x.

Breidenbach, J., Granhus, A., Hylen, G., Eriksen, R., Astrup, R., 2020. A century of National Forest Inventory in Norway – informing past, present, and future decisions. Forest Ecosystems 7 (1), 46. https://doi.org/10.1186/s40663-020-00261-0.

Breiman, L., 2001. Random forests. Machine Learning 45 (1), 5–32. https://doi.org/10.1023/a:1010933404324.

Brooks, E.B., Wynne, R.H., Thomas, V.A., Blinn, C.E., Coulston, J.W., 2014. On-the-Fly Massively Multitemporal Change Detection Using Statistical Quality Control Charts and Landsat Data. IEEE Trans. Geosci. Remote Sens. 52 (6), 3316–3332. https://doi.org/10.1109/TGRS.2013.2272545.

Brown, J. F., Tollerud, H. J., Barber, C. P., Zhou, Q., Dwyer, J. L., Vogelmann, J. E., Loveland, T. R., Woodcock, C. E., Stehman, S. V., Zhu, Z., Pengra, B. W., Smith, K., Horton, J. A., Xian, G., Auch, R. F., Sohl, T. L., Sayler, K. L., Gallant, A. L., Zelenak, D., … Rover, J. (2020). Lessons learned implementing an operational continuous United States national land change monitoring capability: The Land Change Monitoring, Assessment, and Projection (LCMAP) approach. *Remote Sensing of Environment*, *238*, 111356. https://doi.org/10.1016/j.rse.2019.111356.

Bullock, E.L., Woodcock, C.E., Olofsson, P., 2020. Monitoring tropical forest degradation using spectral unmixing and Landsat time series analysis. Remote Sens. Environ. 238, 110968 https://doi.org/10.1016/j.rse.2018.11.011.

Chen, S., Woodcock, C.E., Bullock, E.L., Arévalo, P., Torchinava, P., Peng, S., Olofsson, P., 2021. Monitoring temperate forest degradation on Google Earth Engine using Landsat time series analysis. Remote Sens. Environ. 265, 112648.

Chirici, G., Giannetti, F., McRoberts, R.E., Travaglini, D., Pecchi, M., Maselli, F., Chiesi, M., Corona, P., 2020. Wall-to-wall spatial prediction of growing stock volume based on Italian National Forest Inventory plots and remotely sensed data. Int. J. Appl. Earth Obs. Geoinf. 84, 101959 https://doi.org/10.1016/j.jag.2019.101959.

Chirici, G., Mura, M., McInerney, D., Py, N., Tomppo, E.O., Waser, L.T., Travaglini, D., McRoberts, R.E., 2016. A meta-analysis and review of the literature on the k-Nearest Neighbors technique for forestry applications that use remotely sensed data. Remote Sens. Environ. 176, 282–294. https://doi.org/10.1016/j.rse.2016.02.001.

Cohen, J., 1960. A Coefficient of Agreement for Nominal Scales. Educ. Psychol. Measur. 20 (1), 37–46. https://doi.org/10.1177/001316446002000104.

Cohen, W.B., Healey, S., Yang, Z., Stehman, S., Brewer, C., Brooks, E., Gorelick, N., Huang, C., Hughes, M., Kennedy, R., Loveland, T., Moisen, G., Schroeder, T., Vogelmann, J., Woodcock, C., Yang, L., Zhu, Z., 2017. How Similar Are Forest Disturbance Maps Derived from Different Landsat Time Series Algorithms? Forests 8 (4), 98. https://doi.org/10.3390/f8040098.

Cohen, W.B., Spies, T.A., 1992. Estimating structural attributes of Douglas-fir/western hemlock forest stands from landsat and SPOT imagery. Remote Sens. Environ. 41 (1), 1–17. https://doi.org/10.1016/0034-4257(92)90056-P.

Cohen, W.B., Yang, Z., Healey, S.P., Kennedy, R.E., Gorelick, N., 2018. A LandTrendr multispectral ensemble for forest disturbance detection. Remote Sens. Environ. 205, 131–140. https://doi.org/10.1016/j.rse.2017.11.015.

Cohen, W.B., Yang, Z., Stehman, S.V., Schroeder, T.A., Bell, D.M., Masek, J.G., Huang, C., Meigs, G.W., 2016. Forest disturbance across the conterminous United States from 1985–2012: The emerging dominance of forest decline. For. Ecol. Manage. 360, 242–252. https://doi.org/10.1016/j.foreco.2015.10.042.

Coops, N.C., Shang, C., Wulder, M.A., White, J.C., Hermosilla, T., 2020. Change in forest condition: Characterizing non-stand replacing disturbances using time series satellite imagery. For. Ecol. Manage. 474, 118370 https://doi.org/10.1016/j.foreco.2020.118370.

Crist, E.P., Cicone, R.C., 1984. Comparisons of the dimensionality and features of simulated Landsat-4 MSS and TM data. Remote Sens. Environ. 14 (1–3), 235–246. https://doi.org/10.1016/0034-4257(84)90018-X.

Davis, R. J., Bell, D. M., Gregory, M. J., Yang, Z., Greogory, A. N., Healey, S. P., & Stratton, A. E. (in press). *Northwest Forest Plan – the first 25 years: Status and trends of late-successional and old-growth forests*. Submitted as a General Technical Report to the U.S. Department of Agriculture, Forest Service, Pacific Northwest Research Station.

Davis, R. J., Ohmann, J. L., Kennedy, R. E., Cohen, W. B., Gregory, M. J., Yang, Z., Roberts, H. M., Gray, A. N., & Spies, T. A. (2015). *Northwest Forest Plan – the first 20 years (1994–2013): Status and trends of late-successional and old-growth forests* (Gen. Tech. Rep. PNW-GTR-911; p. 120). U.S. Department of Agriculture, Forest Service, Pacific Northwest Research Station.

Derwin, J.M., Thomas, V.A., Wynne, R.H., Coulston, J.W., Liknes, G.C., Bender, S., Blinn, C.E., Brooks, E.B., Ruefenacht, B., Benton, R., Finco, M.V., Megown, K., 2020. Estimating tree canopy cover using harmonic regression coefficients derived from multitemporal Landsat data. Int. J. Appl. Earth Obs. Geoinf. 86, 101985 https://doi.org/10.1016/j.jag.2019.101985.

Eskelson, B.N.I., Temesgen, H., Lemay, V., Barrett, T.M., Crookston, N.L., Hudak, A.T., 2009. The roles of nearest neighbor methods in imputing missing data in forest inventory and monitoring databases. Scand. J. For. Res. 24 (3), 235–246. https://doi.org/10.1080/02827580902870490.

Foga, S., Scaramuzza, P.L., Guo, S., Zhu, Z., Dilley, R.D., Beckmann, T., Schmidt, G.L., Dwyer, J.L., Joseph Hughes, M., Laue, B., 2017. Cloud detection algorithm comparison and validation for operational Landsat data products. Remote Sens. Environ. 194, 379–390. https://doi.org/10.1016/j.rse.2017.03.026.

Gensiruk, S.A., 1992. Forests of Ukraine. Naukova dumka, Kyiv in Ukrainian.

Gómez, C., White, J.C., Wulder, M.A., 2016. Optical remotely sensed time series data for land cover classification: A review. ISPRS J. Photogramm. Remote Sens. 116, 55–72. https://doi.org/10.1016/j.isprsjprs.2016.03.008.

Griffiths, P., Kuemmerle, T., Baumann, M., Radeloff, V.C., Abrudan, I.V., Lieskovsky, J., Munteanu, C., Ostapowicz, K., Hostert, P., 2014. Forest disturbances, forest recovery, and changes in forest types across the Carpathian ecoregion from 1985 to 2010 based on Landsat image composites. Remote Sens. Environ. 151, 72–88. https://doi.org/10.1016/j.rse.2013.04.022.

Hansen, M.C., Potapov, P.V., Moore, R., Hancher, M., Turubanova, S.A., Tyukavina, A., Thau, D., Stehman, S.V., Goetz, S.J., Loveland, T.R., Kommareddy, A., Egorov, A., Chini, L., Justice, C.O., Townshend, J.R.G., 2013. High-Resolution Global Maps of 21st-Century Forest Cover Change. Science 342 (6160), 850–853. https://doi.org/10.1126/science.1244693.

Henderson, E.B., Bell, D.M., Gregory, M.J., 2019. Vegetation mapping to support greater sage-grouse habitat monitoring and management: Multi- or univariate approach? Ecosphere 10 (8). https://doi.org/10.1002/ecs2.2838.

Henderson, E.B., Ohmann, J.L., Gregory, M.J., Roberts, H.M., Zald, H., Goslee, S., 2014. Species distribution modelling for plant communities: Stacked single species or multivariate modelling approaches? Appl. Veg. Sci. 17 (3), 516–527.

Hermosilla, T., Wulder, M.A., White, J.C., Coops, N.C., Hobart, G.W., 2015. Regional detection, characterization, and attribution of annual forest change from 1984 to 2012 using Landsat-derived time-series metrics. Remote Sens. Environ. 170, 121–132. https://doi.org/10.1016/j.rse.2015.09.004.

Hermosilla, T., Wulder, M.A., White, J.C., Coops, N.C., Hobart, G.W., 2018. Disturbance-Informed Annual Land Cover Classification Maps of Canada's Forested Ecosystems for a 29-Year Landsat Time Series. Canadian Journal of Remote Sensing 44 (1), 67–87. https://doi.org/10.1080/07038992.2018.1437719.

Hermosilla, T., Wulder, M.A., White, J.C., Coops, N.C., Hobart, G.W., Campbell, L.B., 2016. Mass data processing of time series Landsat imagery: Pixels to data products for forest monitoring. Int. J. Digital Earth 9 (11), 1035–1054. https://doi.org/10.1080/17538947.2016.1187673.

Hislop, S., Jones, S., Soto-Berelov, M., Skidmore, A., Haywood, A., Nguyen, T.H., 2019. A fusion approach to forest disturbance mapping using time series ensemble techniques. Remote Sens. Environ. 221, 188–197. https://doi.org/10.1016/j.rse.2018.11.025.

Holubchak, O.I., Hudyma, V.M., Hudyma, V.D., 2018. Forest use in Carpathians: History, present, problems, ways of solution. Proceedings of the International Conference: Main Problems and Tendencies of Further Development of Forestry in the Ukrainian Carpathians in Ukrainian.

Huang, C., Goward, S.N., Masek, J.G., Thomas, N., Zhu, Z., Vogelmann, J.E., 2010. An automated approach for reconstructing recent forest disturbance history using dense Landsat time series stacks. Remote Sens. Environ. 114 (1), 183–198. https://doi.org/10.1016/j.rse.2009.08.017.

Hudak, A.T., Crookston, N.L., Evans, J.S., Hall, D.E., Falkowski, M.J., 2008. Nearest neighbor imputation of species-level, plot-scale forest structure attributes from LiDAR data. Remote Sens. Environ. 112 (5), 2232–2245. https://doi.org/10.1016/j.rse.2007.10.009.

Kashpor, S. M., & Strochynskyi, A. A. (Eds.). (2013). *Forest Inventory Handbook*. Kyiv: Vinichenko, 496 [in Ukrainian].

Kennedy, R.E., Ohmann, J., Gregory, M., Roberts, H., Yang, Z., Bell, D.M., Kane, V., Hughes, M.J., Cohen, W.B., Powell, S., Neeti, N., Larrue, T., Hooper, S., Kane, J., Miller, D.L., Perkins, J., Braaten, J., Seidl, R., 2018a. An empirical, integrated forest biomass monitoring system. Environ. Res. Lett. 13 (2), 025004 https://doi.org/10.1088/1748-9326/aa9d9e.

Kennedy, R.E., Yang, Z., Cohen, W.B., 2010. Detecting trends in forest disturbance and recovery using yearly Landsat time series: 1. LandTrendr – Temporal segmentation algorithms. Remote Sens. Environ. 114 (12), 2897–2910. https://doi.org/10.1016/j.rse.2010.07.008.

Kennedy, R.E., Yang, Z., Gorelick, N., Braaten, J., Cavalcante, L., Cohen, W.B., Healey, S., 2018b. Implementation of the LandTrendr Algorithm on Google Earth Engine. Remote Sensing 10 (5), 691. https://doi.org/10.3390/rs10050691.

Key, C. H., & Benson, N. C. (2006). *Landscape Assessment (LA): Sampling and Analysis Methods* (General Technical Report RMRS-GTR-164; FIREMON: Fire Effects Monitoring and Inventory System, p. LA-1-LA-51). Rocky Mountain Research Station, US Department of Agriculture, Forest Service.

Kuemmerle, T., Chaskovskyy, O., Knorn, J., Radeloff, V. C., Kruhlov, I., Keeton, W. S., & Hostert, P. (2009). Forest cover change and illegal logging in the Ukrainian Carpathians in the transition period from 1988 to 2007. *Remote Sensing of Environment*, *113*(6), 1194–1207. https://doi.org/10.1016/j.rse.2009.02.006.

Kuemmerle, T., Olofsson, P., Chaskovskyy, O., Baumann, M., Ostapowicz, K., Woodcock, C.E., Houghton, R.A., Hostert, P., Keeton, W.S., Radeloff, V.C., 2011. Post-Soviet farmland abandonment, forest recovery, and carbon sequestration in western Ukraine. Glob. Change Biol. 17 (3), 1335–1349. https://doi.org/10.1111/j.1365-2486.2010.02333.x.

Lakyda, P., Shvidenko, A., Bilous, A., Myroniuk, V., Matsala, M., Zibtsev, S., Schepaschenko, D., Holiaka, D., Vasylyshyn, R., Lakyda, I., Diachuk, P., Kraxner, F., 2019. Impact of Disturbances on the Carbon Cycle of Forest Ecosystems in Ukrainian Polissya. Forests 10 (4), 337. https://doi.org/10.3390/f10040337.

Lister, A.J., Andersen, H., Frescino, T., Gatziolis, D., Healey, S., Heath, L.S., Liknes, G.C., McRoberts, R., Moisen, G.G., Nelson, M., Riemann, R., Schleeweis, K., Schroeder, T. A., Westfall, J., Wilson, B.T., 2020. Use of Remote Sensing Data to Improve the Efficiency of National Forest Inventories: A Case Study from the United States National Forest Inventory. Forests 11 (12), 1364. https://doi.org/10.3390/f11121364.

Matasci, G., Hermosilla, T., Wulder, M.A., White, J.C., Coops, N.C., Hobart, G.W., Bolton, D.K., Tompalski, P., Bater, C.W., 2018a. Three decades of forest structural dynamics over Canada's forested ecosystems using Landsat time-series and lidar plots. Remote Sens. Environ. 216, 697–714. https://doi.org/10.1016/j.rse.2018.07.024.

Matasci, G., Hermosilla, T., Wulder, M.A., White, J.C., Coops, N.C., Hobart, G.W., Zald, H.S.J., 2018b. Large-area mapping of Canadian boreal forest cover, height, biomass and other structural attributes using Landsat composites and lidar plots. Remote Sens. Environ. 209, 90–106. https://doi.org/10.1016/j.rse.2017.12.020.

Matsala, M., Bilous, A., Myroniuk, V., Diachuk, P., Burianchuk, M., Zadorozhniuk, R., 2021a. Natural forest regeneration in Chernobyl Exclusion Zone: Predictive mapping and model diagnostics. Scand. J. For. Res. 36 (2-3), 164–176.

Matsala, M., Bilous, A., Myroniuk, V., Holiaka, D., Schepaschenko, D., See, L., Kraxner, F., 2021b. The Return of Nature to the Chernobyl Exclusion Zone: Increases in Forest Cover of 1.5 Times Since the 1986 Disaster. Forests 12 (8), 1024. https://doi.org/10.3390/f12081024.

McRoberts, R.E., 2009. Diagnostic tools for nearest neighbors techniques when used with satellite imagery. Remote Sens. Environ. 113 (3), 489–499. https://doi.org/10.1016/j.rse.2008.06.015.

McRoberts, R.E., 2012. Estimating forest attribute parameters for small areas using nearest neighbors techniques. For. Ecol. Manage. 272, 3–12. https://doi.org/10.1016/j.foreco.2011.06.039.

McRoberts, R.E., Tomppo, E.O., Næsset, E., 2010. Advances and emerging issues in national forest inventories. Scand. J. For. Res. 25 (4), 368–381. https://doi.org/10.1080/02827581.2010.496739.

Moeur, M., Stage, A.R., 1995. Most similar neighbor—An improved sampling inference procedure for natural-resource planning. Forest Science 41 (2), 337–359.

Myroniuk, V., Kutia, M., Sarkissian, A.J., Bilous, A., Liu, S.h., 2020. Regional-Scale Forest Mapping over Fragmented Landscapes Using Global Forest Products and Landsat Time Series Classification. Remote Sensing 12 (1), 187. https://doi.org/10.3390/rs12010187.

Nguyen, T.H., Jones, S.D., Soto-Berelov, M., Haywood, A., Hislop, S., 2018a. A spatial and temporal analysis of forest dynamics using Landsat time-series. Remote Sens. Environ. 217, 461–475. https://doi.org/10.1016/j.rse.2018.08.028.

Nguyen, T.H., Jones, S.D., Soto-Berelov, M., Haywood, A., Hislop, S., 2020. Monitoring aboveground forest biomass dynamics over three decades using Landsat time-series and single-date inventory data. Int. J. Appl. Earth Obs. Geoinf. 84, 101952 https://doi.org/10.1016/j.jag.2019.101952.

Nguyen, T.H., Jones, S., Soto-Berelov, M., Haywood, A., Hislop, S., 2018b. A Comparison of Imputation Approaches for Estimating Forest Biomass Using Landsat Time-Series and Inventory Data. Remote Sensing 10 (11), 1825. https://doi.org/10.3390/rs10111825.

Nita, M.D., Munteanu, C., Gutman, G., Abrudan, I.V., Radeloff, V.C., 2018. Widespread forest cutting in the aftermath of World War II captured by broad-scale historical Corona spy satellite photography. Remote Sens. Environ. 204, 322–332. https://doi.org/10.1016/j.rse.2017.10.021.

Ohmann, J.L., Gregory, M.J., 2002. Predictive mapping of forest composition and structure with direct gradient analysis and nearest- neighbor imputation in coastal Oregon, U.S.A. Can. J. For. Res. 32 (4), 725–741. https://doi.org/10.1139/x02-011.

Ohmann, J.L., Gregory, M.J., Roberts, H.M., 2014. Scale considerations for integrating forest inventory plot data and satellite image data for regional forest mapping. Remote Sens. Environ. 151, 3–15. https://doi.org/10.1016/j.rse.2013.08.048.

Ohmann, J.L., Gregory, M.J., Roberts, H.M., Cohen, W.B., Kennedy, R.E., Yang, Z., 2012. Mapping change of older forest with nearest-neighbor imputation and Landsat time-series. For. Ecol. Manage. 272, 13–25. https://doi.org/10.1016/j.foreco.2011.09.021.

Oliinyk, Y.e., 2019. Forestry in Ukraine 2019. Analytical Study. Kyiv. Civic Union "Bioenergy Association of Ukraine" (in Ukrainian), p. (p. 38)..

Olofsson, P., Foody, G.M., Herold, M., Stehman, S.V., Woodcock, C.E., Wulder, M.A., 2014. Good practices for estimating area and assessing accuracy of land change. Remote Sens. Environ. 148, 42–57. https://doi.org/10.1016/j.rse.2014.02.015.

Orsi, F., Ciolli, M., Primmer, E., Varumo, L., Geneletti, D., 2020. Mapping hotspots and bundles of forest ecosystem services across the European Union. Land Use Policy 99, 104840. https://doi.org/10.1016/j.landusepol.2020.104840.

Pflugmacher, D., Cohen, W. B., & E. Kennedy, R. (2012). Using Landsat-derived disturbance history (1972–2010) to predict current forest structure. *Remote Sensing of Environment*, *122*, 146–165. https://doi.org/10.1016/j.rse.2011.09.025.

Phalan, B.T., Northrup, J.M., Yang, Z., Deal, R.L., Rousseau, J.S., Spies, T.A., Betts, M.G., 2019. Impacts of the Northwest Forest Plan on forest composition and bird populations. Proc. Natl. Acad. Sci. 116 (8), 3322–3327. https://doi.org/10.1073/pnas.1813072116.

Potapov, P.V., Turubanova, S.A., Tyukavina, A., Krylov, A.M., McCarty, J.L., Radeloff, V. C., Hansen, M.C., 2015. Eastern Europe's forest cover dynamics from 1985 to 2012 quantified from the full Landsat archive. Remote Sens. Environ. 159, 28–43. https://doi.org/10.1016/j.rse.2014.11.027.

Riemann, R., Wilson, B.T., Lister, A., Parks, S., 2010. An effective assessment protocol for continuous geospatial datasets of forest characteristics using USFS Forest Inventory and Analysis (FIA) data. Remote Sens. Environ. 114 (10), 2337–2352. https://doi.org/10.1016/j.rse.2010.05.010.

Roy, D.P., Kovalskyy, V., Zhang, H.K., Vermote, E.F., Yan, L., Kumar, S.S., Egorov, A., 2016. Characterization of Landsat-7 to Landsat-8 reflective wavelength and normalized difference vegetation index continuity. Remote Sens. Environ. 185, 57–70. https://doi.org/10.1016/j.rse.2015.12.024.

Schroeder, T.A., Schleeweis, K.G., Moisen, G.G., Toney, C., Cohen, W.B., Freeman, E.A., Yang, Z., Huang, C., 2017. Testing a Landsat-based approach for mapping disturbance causality in U.S. forests. Remote Sens. Environ. 195, 230–243. https://doi.org/10.1016/j.rse.2017.03.033.

Senf, C., Pflugmacher, D., Hostert, P., Seidl, R., 2017. Using Landsat time series for characterizing forest disturbance dynamics in the coupled human and natural systems of Central Europe. ISPRS J. Photogramm. Remote Sens. 130, 453–463. https://doi.org/10.1016/j.isprsjprs.2017.07.004.

Senf, C., Seidl, R., 2021. Mapping the forest disturbance regimes of Europe. Nat. Sustainability 4 (1), 63–70. https://doi.org/10.1038/s41893-020-00609-y.

Soulard, C.E., Acevedo, W., Cohen, W.B., Yang, Z., Stehman, S.V., Taylor, J.L., 2017. Harmonization of forest disturbance datasets of the conterminous USA. Environ.

Monit. Assess. 189 (4) https://doi.org/10.1007/s10661-017-5879-5 from 1986 to 2011.

Souza, C.M., Roberts, D.A., Cochrane, M.A., 2005. Combining spectral and spatial information to map canopy damage from selective logging and forest fires. Remote Sens. Environ. 98 (2–3), 329–343. https://doi.org/10.1016/j.rse.2005.07.013.

Stefanski, J., Chaskovskyy, O., Waske, B., 2014. Mapping and monitoring of land use changes in post-Soviet western Ukraine using remote sensing data. Appl. Geogr. 55, 155–164. https://doi.org/10.1016/j.apgeog.2014.08.003.

Storozhuk, V., Polley, H., 2017. Forest Inventory—Status Quo in Ukraine, Experience of Germany, and FAO Recommendations (Agricultural Policy Report APD/APB/06/2017; German-Ukrainian Agricultural Policy. in Ukrainian Dialogue. p. 52). https://www.apd-ukraine.de/images/2018/APR/APD_APR_07-2017_Forest_Inventories_ukr.pdf.

ter Braak, C.J.F., 1986. Canonical Correspondence Analysis: A New Eigenvector Technique for Multivariate Direct Gradient Analysis. Ecology 67 (5), 1167–1179. https://doi.org/10.2307/1938672.

Tomppo, E. (1990). Designing a satellite image-aided National Forest Survey in Finland. Proceedings of the SNS/IUFRO Workshop on the Usability of Remote Sensing for Forest Inventory and Planning, 26–28, Feb. 1990. Umeå. Sweden. International Union of Forest Research Organizations, Vienna, pp. 43–47.

Tomppo, E., Gschwantner, T., Lawrence, M., & McRoberts, R. E. (Eds.). (2010). *National forest inventories: Pathways for common reporting.* Springer.

Weiss, A. (2001). *Topographic Position and Landforms Analysis.* [Poster presentation]. ESRI User Conference, San Diego, CA.

Wilson, B.T., Knight, J.F., McRoberts, R.E., 2018. Harmonic regression of Landsat time series for modeling attributes from national forest inventory data. ISPRS J. Photogramm. Remote Sens. 137, 29–46. https://doi.org/10.1016/j.isprsjprs.2018.01.006.

Wilson, B. T., Lister, A. J., & Riemann, R. I. (2012). A nearest-neighbor imputation approach to mapping tree species over large areas using forest inventory plots and moderate resolution raster data. *Forest Ecology and Management*, *271*, 182–198. https://doi.org/10.1016/j.foreco.2012.02.002.

Wulder, M.A., Loveland, T.R., Roy, D.P., Crawford, C.J., Masek, J.G., Woodcock, C.E., Allen, R.G., Anderson, M.C., Belward, A.S., Cohen, W.B., Dwyer, J., Erb, A., Gao, F., Griffiths, P., Helder, D., Hermosilla, T., Hipple, J.D., Hostert, P., Hughes, M.J., Huntington, J., Johnson, D.M., Kennedy, R., Kilic, A., Li, Z., Lymburner, L., McCorkel, J., Pahlevan, N., Scambos, T.A., Schaaf, C., Schott, J.R., Sheng, Y., Storey, J., Vermote, E., Vogelmann, J., White, J.C., Wynne, R.H., Zhu, Z., 2019. Current status of Landsat program, science, and applications. Remote Sens. Environ. 225, 127–147.

Wulder, M.A., Masek, J.G., Cohen, W.B., Loveland, T.R., Woodcock, C.E., 2012. Opening the archive: How free data has enabled the science and monitoring promise of Landsat. Remote Sens. Environ. 122, 2–10. https://doi.org/10.1016/j.rse.2012.01.010.

Ye, S., Rogan, J., Zhu, Z., Eastman, J.R., 2021a. A near-real-time approach for monitoring forest disturbance using Landsat time series: Stochastic continuous change detection. Remote Sens. Environ. 252, 112167 https://doi.org/10.1016/j.rse.2020.112167.

Ye, S., Rogan, J., Zhu, Z., Hawbaker, T.J., Hart, S.J., Andrus, R.A., Meddens, A.J.H., Hicke, J.A., Eastman, J.R., Kulakowski, D., 2021b. Detecting subtle change from dense Landsat time series: Case studies of mountain pine beetle and spruce beetle disturbance. Remote Sens. Environ. 263, 112560 https://doi.org/10.1016/j.rse.2021.112560.

Zald, H.S.J., Wulder, M.A., White, J.C., Hilker, T., Hermosilla, T., Hobart, G.W., Coops, N.C., 2016. Integrating Landsat pixel composites and change metrics with lidar plots to predictively map forest structure and aboveground biomass in Saskatchewan, Canada. Remote Sens. Environ. 176, 188–201. https://doi.org/10.1016/j.rse.2016.01.015.

Zhu, Z., Woodcock, C.E., 2014. Continuous change detection and classification of land cover using all available Landsat data. Remote Sens. Environ. 144, 152–171. https://doi.org/10.1016/j.rse.2014.01.011.

Zhu, Z., Zhang, J., Yang, Z., Aljaddani, A.H., Cohen, W.B., Qiu, S., Zhou, C., 2020. Continuous monitoring of land disturbance based on Landsat time series. Remote Sens. Environ. 238, 111116 https://doi.org/10.1016/j.rse.2019.03.009.